https://doi.org/10.1016/j.jcsr.2016.06.016
This is the Pre-Published Version.

Design for Inelastic Local Web Buckling of Coped Beams

Angus C.C. Lam[a], Yanyang Zhang[b*], Yi Qin[a], Michael C.H. Yam[b], and V.P. Iu[a]

[a)] *Department of Civil & Environmental Engineering, University of Macau, Macau SAR, China*
[b)] *Department of Building & Real Estate, The Hong Kong Polytechnic University, Hung Hom, Kowloon, Hong Kong SAR, China*
**Corresponding author: email: yanyang.zhang@polyu.edu.hk, Tel: +852 2766 8130*

Abstract

This paper presents a numerical study on the inelastic local web buckling behaviour of top flange coped beams with welded end connections. The modelling strategy based on the finite element (FE) method was validated and calibrated using the test results obtained in previous experimental work. Subsequently, a comprehensive parametric study using the validated FE model was carried out to carefully examine the effects of various parameters on the inelastic buckling strength and behaviour of practical coped beams with a welded end plate connection. Evident inelastic buckling behaviour was observed in most of the FE models, except for those with web slenderness (d/t_w) equal to 56.3 and cope length to reduced beam depth ratio (c/h_0) equal to 1.0. The influence of initial geometric imperfection on the buckling strength and response was also investigated in detail. Based on the parametric study results, a design approach according to the 'plate shear buckling model' was proposed to evaluate the inelastic buckling strength of coped beams. It was shown that the proposed approach provided better predictions of the FE results when compared with those of the current design strategy.

Keywords: Coped beams; inelastic local web buckling; finite element analysis; design approach

1. Introduction

In steel construction, secondary beams are usually connected to the main girder using simple welded or bolted connections with single/double clip angles, fin plates or end plates. In order to provide sufficient clearance at the connections, the flanges are often coped at the beam ends, as shown in Fig. 1. Depending on the construction and the architectural requirements, beams can be coped at the top flange, the bottom flange or both flanges. Moreover, due to the presence of copes, local failures including flexural yielding, shear yielding, local web buckling and block shear are more prone to happen in such beam ends compared with the uncoped beam sections.

Local web buckling failure may occur in the vicinity of the cope because of the removal of the flange(s) of the beam, particularly for coped beams with a relatively large cope length to reduced web depth ratio (c/h_0 – see Fig. 1) and a small web thickness [1]. The local web buckling behaviour of coped beams with bolted end connections was studied by a number of researchers in the late 1970s and early 1980s on beam web shear connections [2-6]. In late 1980s, Cheng and his colleagues [1, 7] investigated experimentally and numerically the local web buckling behaviour of coped beams with an end plate connection. They [1, 7] carried out ten tests on top flange coped beams to check the reliability of the proposed design equations, five of which were designed to fail by inelastic buckling, while the other five failed by elastic buckling. It was observed that in the elastic buckling cases, linear behaviour governed the initial stage of the beam load-deflection response until the sudden drop of the loading capacity due to the occurrence of local web buckling. In the inelastic buckling case, however, a nonlinear load-deflection response was observed before buckling happened indicating that initial yielding occurred prior to web buckling. In addition, Cheng et al. [1] stated that the inelastic local buckling strength of coped beams usually does not control the design since either the flexural yield strength or the shear strength of the coped beam section always

provides a lower bound capacity of the connection. Followed up with Cheng's work [1, 7], Yam and his colleagues [8-17] carried out a series of research on coped I beams with welded and bolted connections with and without stiffeners. Yam et al. [17] performed four tests on welded I beam sections to further study the local web buckling behaviour of top flange coped beams. All the test specimens [17] were found failed by local web buckling at the cope region. The experimental and numerical results from [17] showed that the buckling line usually inclined at an angle of about 45° in the beam web. Based on the research findings in [17], Yam et al. proposed an alternative design equation towards the elastic local web buckling of coped beams based on a plate shear buckling model. Compared with Cheng's equations [7], the new design equation provides a better prediction of the elastic local web buckling strength of coped beams. In [8], a total of ten tests on top flange coped beams with welded clip angle connections were conducted to examine the block shear strength and behaviour, in which five test specimens with relative small c/h_0 ratio (smaller than 0.4) were found failed by inelastic local web buckling. The test results [8] showed that the web plate of the five test specimens usually buckled at the end of the cope, where severe compression and shear yielding was initiated before the ultimate load was reached. The results [8] also showed that inelastic local web buckling was a potential failure mode for coped beams with welded clip angel connections. More recently, Aalberg [18, 19] conducted a series of tests on the local web buckling of top flange coped I beams fabricated using hot-rolled S355 and aluminium materials. In [19], six tests were performed to study the buckling capacity of top flange coped steel beams, in which one test was on uncoped beam and the remaining five were on coped beams with different cope geometry. Compared with the previous research [1, 8], the test specimens [19] did not have lateral support and rotational restraint along the vertical edge of the web at the beam end. The test results [19] showed that both the uncoped beam S1 and the coped beam S2 (c/h_0 = 0.53) were failed by compressive web buckling at the supported region.

The remaining four specimens S3-S6 with relatively large c/h_0 ratio (1.06, 1.59, 0.87 and 1.34 respectively) were failed by inelastic local web buckling, which was developed around the cope corner and almost across the entire beam depth. Through the comparison between the test results [19] and predictions obtained from Cheng's method [7] and Yam's method [17], it was found that the shear model proposed by Yam et al. [17] provided the best buckling predictions, although non-conservative estimates were obtained for specimens S2 and S5. This was due to the fact that the boundary conditions of Cheng's model [7] and Yam's model [17] are different from those of Aalberg's test specimens [19].

Based on the above discussions, a design strategy for assessing the local capacity of coped beam end was proposed by Yam et al. [16] which is based on the lowest value of ultimate beam reactions calculated according to the critical bending stress (σ_{cr}) from Cheng's method [7], the critical shear stress (τ_{cr}) from Yam's method [17], the bending yield strength (R_y) and the shear yield strength (R_{vy}) of the coped section. However, depending on the cope details and the grade of steel used in fabricating the coped beams, inelastic local web buckling of coped beams may govern the design instead of the bending or shear yielding behaviour at the coped beam section. As most of the previous research focused on the elastic local web buckling of top flange coped beams, the inelastic local web buckling response has not been adequately investigated. Hence, the objective of the study is to investigate numerically the inelastic local web buckling behaviour of coped beams and to propose a corresponding design approach for practical beam sections. The research findings of the local web buckling of coped beams including both test and numerical results obtained from past research studies [1, 7-9] were used to validate a finite element (FE) model of coped beam. A comprehensive parametric study on the inelastic web buckling strength and behaviour of coped beams based on the validated FE model was performed subsequently. It should be noted that only top flange (compression flange) coped beams with welded end plate connections were studied. Finally,

based on the existing test results from the literature and the parametric study results from this study, a design equation for evaluating the inelastic local web buckling of top flange coped beams with welded end plate connections was proposed.

2. Current design equations for local web buckling of coped beams

As mentioned, Cheng [1, 7] proposed a set of design equations to evaluate the elastic local web buckling of coped beam and this design recommendation was adopted by the AISC Steel Construction Manual [20]. Cheng's design model is based on the classical plate buckling model with assumed simplified boundary conditions. It was assumed that the top edge of the plate was free and the other three edges were simply supported, as shown in Fig. 2a. With the assumption of a linear stress distribution, the elastic buckling stress (the maximum stress at the top of the cope), is expressed by

$$\sigma_{cr} = k\frac{f\pi^2 E}{12\left(1-v^2\right)}\left(\frac{t_w}{h_o}\right)^2 \tag{1}$$

where E = Young's modulus, υ = Poisson's ratio, t_w = web thickness, h_0 = reduced beam depth at the coped region. The plate buckling coefficient k is given by:

$$k = 2.2\left(\frac{h_0}{c}\right)^{1.65} \quad \text{for } \frac{h_0}{c} \le 1$$

$$k = 2.2\left(\frac{h_0}{c}\right) \quad \text{for } \frac{h_0}{c} > 1$$

where c = cope length (Fig. 1) and the adjustment factor f is defined as

$$f = \frac{2c}{D} \quad \text{for } \frac{c}{D} \le 1$$

$$f = 1 + \frac{c}{D} \quad \text{for } \frac{c}{D} > 1$$

where D = beam depth.

On the other hand, Yam's method [17] was based on a plate shear buckling model which reflects more realistically the buckling behaviour of the coped region observed from the test results (see Fig.2b). The corresponding critical shear stress τ_{cr} is expressed by,

$$\tau_{cr} = k_s \frac{\pi^2 E}{12\left(1-\nu^2\right)}\left(\frac{t_w}{h_o}\right)^2 \tag{2}$$

where k_s is the shear buckling coefficient, given by

$$k_s = a\left(\frac{h_0}{c}\right)^b,$$

where $a = 1.38 - 1.79\frac{d_c}{D}$, and $b = 3.64\left(\frac{d_c}{D}\right)^2 - 3.36\frac{d_c}{D} + 1.55$.

In design practice, the above critical bending stress (σ_{cr}) and critical shear stress (τ_{cr}) should not exceed the design bending stress (σ_b) and shear stress (τ_s) calculated from conventional beam theory, which are expressed by $\sigma_b = \frac{M}{S}$ and $\tau_s = \frac{V}{t_w h_0}$, where M = bending moment, S = elastic section modulus, and V = shear force. Additionally, the Steel Construction Institute (SCI) [21] states that local web buckling checking of coped end is not required when the cope length is less than $110{,}000D/(D/t_w)^3$, for $D/t_w > 48$ (Grade 50 steel, $\sigma_y \geq 325$MPa) or $d_c < D/2$ and $c < D$, for $D/t_w < 48$ for S355 steel.

For the design against inelastic local web buckling of single flange coped beams, the design capacity of coped beam end (R_{design}) can be expressed by R_{design} = minimum of R_{cr}, R_{vy}, and R_y, in which R_{cr} represents the elastic buckling strength and is given by

$$R_{cr} = \text{minimum of } R_{cheng}(\sigma_{cr} h_0 t) \text{ and } R_{yam}(\tau_{cr} h_0 t_w) \tag{3}$$

where, R_{cheng} and R_{yam} are the ultimate beam reactions calculated based on the critical bending stress (σ_{cr}) and critical shear stress (τ_{cr}) respectively. The shear yield strength of the coped section (T section) for the coped region is given by

$$R_{vy} = 0.6 f_y h_0 t_w \tag{4}$$

where f_y = the material yield strength.

The bending yield strength is expressed by:

$$R_y = \frac{f_y I_c}{y_c c} \tag{5}$$

where I_c = the second moment of area of the coped section, and y_c = the distance from the neutral axis to the top edge of the coped region.

3. Tests performed by Cheng et al. [1] and Yam et al. [8]

Cheng et al. [1] conducted a series of full-scale tests to examine the strength and behaviour of single (top) flange coped steel beams with welded double clip angle connections. In the tests, two specimens (namely, W1 and W2) were failed by inelastic local web buckling. The test beams were fabricated from 3.048m long W18×35 sections using A36 material. Two types of clip angle fabricated using 10mm steel plates were employed in the tests [1]. The clip angles were welded to the coped end of the beam web and the connection was bolted to the supporting column. A roller support was used for the other end of the test beams. Lateral bracings were provided near the load and reaction positions, and at the end of the copes. A monotonic concentrated load through a hydraulic ram was applied to the test beams at a location approximately 610mm from the supporting columns. More detailed description of the test programme and the test results can be found in [1].

More recently, Yam et al. [8] carried out ten full-scale tests to investigate the block shear strength and behaviour of single (top) flange coped beams, in which six specimens A1, A2, B1, B2, D1, and E2 were failed by inelastic local web buckling at the coped end. The test beams were 3.3m long and fabricated from three different section sizes of UB406×140×46 (6.8mm), UB457×191×74 (9.2mm) and UB356×171×67 (9.1mm) with different web thickness. Double clip angles with a thickness of 16mm and five different web block aspect ratios were used in the connections. The web block aspect ratio is defined as the ratio of vertical shear area (p+b)

to the horizontal tension area (a) of the beam web, as illustrated in Table 1. The test programme was similar to those performed by Cheng et al. [1]. The double clip angles were welded to the coped end of the specimens and connected to a fixed stud column using 24mm diameter bolts, while the other beam end was supported by a roller. Bracing systems were placed at the loading position, the support, and at the top flange of the beam near the coped end. Vertical loads were applied monotonically to the test beams by a hydraulic ram. The chosen loading position for beam A, B, D and E was 510mm, 510mm, 600mm and 550mm, respectively, from the stud column. More detailed description of the specimens and test setup can be found in [8].

The in-plane deflections of all the eight specimens were measured at the loading position, while strain readings were recorded in the coped region of the beam web. The dimensions and the cope details of the specimens are illustrated in Table 1, while the steel materials properties of the specimens are summarized in Table 2. A summary of the experimental results is shown in Table 3, where the ultimate reaction forces, R_{ex} at the beam support and the failure mode of the specimens are provided. It was found that all the eight specimens were failed by inelastic local web buckling due to the combined bending and shear in the coped region. In the tests performed by Cheng et al. [1], it was found that the ultimate reactions at the coped end obtained from specimen W2 with a larger cope length was slightly lower than that of specimen W1 which has a shorter cope length. In the tests performed by Yam et al. [8], specimens A1, A2, B1, B2, D1, and E2 had a web block aspect ratio of 3.6, 2.3, 2.8, 1.4, 1.6 and 3.3, respectively. The test results indicated that the buckling capacity of the coped beam specimens increased with increasing web block aspect ratio. As mentioned, the aspect ratio was associated with the ratio of the shear area (b) and the tension area (a) of the beam web, as illustrated in Table 1. When the tension area (a) was increased, the loading eccentricity between the centroid of the connection to the column face was also increased correspondingly

and therefore generated more secondary bending to the web edge near the clip angles at the coped end. The load-deflection behaviour of the specimens, are presented later in Section 4. More detail discussions of the test results can be found in [1] and [8].

4. Finite element analysis of the test specimens

4.1 General

A numerical study of the abovementioned test specimens is presented here to offer a more thorough understanding of the local web buckling behaviour of coped steel beams and help explain the test results. More importantly, the nonlinear FE model validated by the test results can be used to conduct a parametric study to carefully examine the inelastic local web buckling strength and behaviour of coped beams. The FE models discussed in this research were established using a general FE package, ABAQUS 6.12 [22], in which both the material and geometric nonlinearities were considered. In order to accurately model the test specimens in the FE analysis, the measured geometrical dimensions and material properties of the specimens obtained in [1, 8] were used. The effect of residual stress within the coped region was not considered in the FE analysis since no residual stress measurements were recorded in the existing test results and it is difficult to estimate the actual residual stress pattern in the coped region for the analysis. Moreover, it is known that the fabrication of cope by flame-cutting procedure would introduce large tensile residual stress in the coped edge because of temperature difference during the cooling process [23, 24]. Hence, it is believed that ignoring the tensile residual stress effect in the vicinity of the coped edge in the FE analysis would be a conservative assumption. Detailed descriptions of the FE modelling techniques are described as follows.

4.2 Modelling strategy

Four-node quadrilateral shell elements (S4R) with reduced integration were used to discretise the steel beams, including the beam web, the flanges and the stiffeners. The S4R shell element is computationally inexpensive and provides accurate solution for structural elements with small thickness. However, the clip angles were modelled using eight-node three dimensional hexahedral elements with reduced-integration (C3D8R) to better consider the clip angle dimensions. A typical FE mesh employed in the current study is shown in Fig. 3. For the beam web in the vicinity of the cope, where local web buckling was expected to occur, a finer mesh was considered and the mesh size became coarse towards the other end of the beam.

A typical isotropic elastic-plastic material model with von Mises yield criterion was employed to represent the material nonlinearity of the steel material. The key material properties, such as the Young's modulus, yield strength, and ultimate strength, were obtained from the tensile coupon test results [8]. The engineering stress and strain relationship for the material was converted to true stress and strain curve employed in the FE models with a linear behaviour in the elastic stage and followed with a multi-linear strain hardening response. Beyond the ultimate stress/strain, a material stiffness of 0.2GPa was assumed based on the study from [25] in order to obtain a reasonable material response beyond the initiation of necking. A typical true stress-true strain response employed in the FE models is shown in Fig. 4.

Since no weld failure was observed in the tests, rigid links, which constrain all degrees of freedom of the two connected nodes, were assumed between the web and the clip angles to simulate the fillet welds. The multi-point constraint (MPC) type BEAM, which provides a rigid beam between two nodes constraining the displacement and rotation of the first node to the second node were used as the rigid link [22]. Two sets of MPC type BEAM, namely Group1 and Group2, were used to link the corresponding nodes on the web and the clip angles, respectively, as shown in Fig. 3b. Group1 was used to constrain the clip angle edge to the

beam web at the weld root, while Group2 was used to constrain all nodes from the centre line of the clip angle thickness to the beam web at the weld leg to take into account the influence of weld size.

Quasi-static loading procedure was applied at the loading position to simulate the applied load, *P* as shown Fig. 3a. Vertical support was applied at the uncoped beam end to simulate the roller assembly in the test. Therefore, only the vertical displacement was constrained (U2 = 0) at the uncoped beam end, while both the rotational and longitudinal movement were allowed. At the coped end, the beam was connected to a supporting column via the double clip angles connections. Six snug-tightened bolts were employed for the connections, and additional washers were used for each bolt to provide sufficient clearance between the angle and column flange face, and thus to minimize the rotational stiffness of connections. The presence of washers between the clip angles and the column flange was simulated using spring elements, which were applied in the horizontal direction (U1), as shown in Fig. 3c. As the support column was not actually simulated in the FE model, spring elements were used to link the nodes around the bolt holes to the 'ground' that represents the rigid column. A total of 36 spring elements were used around each bolt hole. Bilinear tensile and compressive spring elements were used to consider the effect of the washers, where the initial stiffness of each spring was taken as 200N/mm at first 0.5mm of deformation, and then 40000N/mm was considered beyond 0.5mm. These spring characteristics were recommended by Yam et al., where a comprehensive parametric study can be found in [9]. The vertical (U2) and lateral (U3) degrees of freedom of the springs were fully restrained. The lateral bracings, which were provided to prevent the test specimens from lateral movement, were considered using lateral restraints (U3 = 0) imposed at the corresponding locations of the beam flanges.

A two-step approach was adopted to examine the inelastic buckling behaviour of the coped beam specimens. The first step was the use of an eigenvalue analysis (buckling analysis) to

obtain the elastic local web buckling mode at the cope. Based on the buckling mode shape from the first step and an assumed initial imperfection magnitude, a nonlinear load deflection analysis of the test specimens was conducted to trace the nonlinear load deflection response of the coped beams. Since no measure initial imperfection magnitude was provided in [1, 8], a trial-and-error process was employed to determine an assumed initial imperfection magnitude. The initial imperfection magnitude was varied until the analytical load deflection curves of the specimens generally agreed well with those from the test results. The assumed initial imperfection magnitudes, which varied between 0.7mm and 3.0mm, for the specimens are summarized in Table 3. A sensitivity study on the influence of imperfection amplitude was also performed, and is discussed later in Section 5.3.

4.3 Results and discussions

The FE results show that the typical failure mode of the coped beam specimens at the coped region is inelastic local web buckling as shown in Figs. 5a and c. In general, the most significant out-of-plane deformation was observed at the cope corner (see Fig. 5a). Yielding was initiated at the cope corner, and then propagated diagonally within the coped region. Eventually, the web was slightly twisted and a 'buckling line (see Fig. 5d)' appeared from the cope corner to the bottom of the beam web at a certain inclined orientation of around 45° to the horizontal. As shown in Fig. 5, the failure modes of the specimens predicted by the FE analysis are generally compared well with those from the test results.

The ultimate reaction forces at the coped end of the specimens predicted by the FE analyses, R_{nu}, are summarised in Table 3 with the assumed initial imperfection values. The test reactions at the cope end of the specimens, R_{ex}, are also provided in the same table for comparison. The test-to-FE ratio (R_{ex}/R_{nu}) varies from 0.96 to 1.03, with a mean value of 0.99. The corresponding coefficient of variation (CoV) is 0.024.

The load-deflection curves of all the eight test specimens from the FE analysis results and the test results are shown in Fig. 6. In general, linear behaviour is observed at the initial stage, while nonlinear response is initiated when the applied loads approaches around 60%-70% of the ultimate loads in all the specimens. The typical failure mode (see Figs. 5a and c) correlating with the load-deflection behaviour (see Figs. 6b and d) offers a clear understanding of the development of inelastic local web buckling of the specimens. For specimen A2, the coped beam remains in the elastic range when the applied load P is below 350kN. Beyond the elastic limit (350kN), buckling is initiated at the cope corner and propagates towards the un-coped section. Beyond the peak load (540kN), web twisting becomes significant, and the applied load drops gradually. In the meantime, significant yielding due to high stress concentration near the cope corner is also observed. Although the initial slope of the FE load deflection curves of specimen D1, E2 and W2 is slightly larger than that of the test curves, the general trend of the load-deflection response is well predicted by the FE analysis.

Furthermore, selected strain gauge results recorded in the tests [8] and the predicted strains from the FE analyses are compared in Fig. 7. In general, the test strain distribution patterns are in reasonable agreement with those obtained from the FE predictions, in terms of trend and the magnitude of the strains. As shown in the figure, the largest tensile strain is found at the beam end and the strain decreased along the tension area. This is due to the effect of loading eccentricity on the connection. Besides, the figure also shows that the strain gradient at lower load level (P = 70kN) is slight smaller than that at the higher load level (P = 183kN).

To further investigate the effects of different parameters on the inelastic local web buckling strength and behaviour of coped beams, a parametric study is presented in the following section.

5. Parametric studies and discussions

5.1 General

A parametric study was carried out to further study the influence of different parameters on the inelastic local web buckling strength and behaviour of coped beams. The FE models employed in the parametric study were based on the ones validated by the previous test results as mentioned above. In all the models, the beam span length, L, was considered as approximately ten times that of the beam depth, D, while the loading position was maintained at a distance of 1.5 times of D from the coped end to minimize the effect of stress concentration in the coped region. As double clip angle connections would provide additional strengthening effect in the coped region, end plate connections were employed instead in the parametric study. The thickness of the end plate was assumed to be 16mm, which was the same as that used in the experimental programme [8]. The modelling strategy used in the model validation was employed in the parametric study, as shown in Fig. 3, and the weld size was assumed to be 10mm. The same property of the spring elements used in the model validation, which linked the nodes of the bolt holes to a 'rigid ground', was used for the end plate connections. In the nonlinear analysis, an initial geometric imperfection of 2.5mm was consistently used in association with the first/fundamental buckling mode. The reason is discussed in detail in Section 5.3. The material model used in the validation process was employed for all the FE models in the parametric study. The modulus of elasticity (E) was taken as 205GPa, and the yield strength (f_y) and ultimate strength (f_u) of the steel material were assumed to be 355MPa and 540MPa, respectively, while the Poisson's ratio was taken as 0.3. The details of the parameters and variables examined in the parametric study are shown in Table 4. As shown in the table, the parameters examined in the study are the ratio of coped length to reduced beam depth, (c/h_0), the ratio of cope depth to beam depth, (d_c/D), and the web slenderness, (d/t_w), where d is the clear distance between the flanges minus the fillet.

Four steel beam sections namely: UB203×133×30, UB610×305×179, UB356×171×51, and UB406×140×39 were examined in the present study. These sections represent a variation of the web slenderness, (d/t_w). Accordingly, the selected web slenderness varied from 26.9 (UB203×133×30) to 56.3 (UB406×140×39) which is the largest web slenderness ratio among the existing universal beam sections. It was reported in [5] that when the cope length and cope depth are relatively short, compared with the beam depth, shear yielding may control the failure behaviour. Thus, three d_c/D ratios (0.05, 0.1 and 0.15), and five c/h_0 ratios (0.1, 0.25, 0.5, 0.75 and 1.0) were examined for each beam section. Totally, sixty FE analyses were performed and the corresponding results are presented in the following sections. For simplicity, the four beam sections UB203, UB610, UB356 and UB406 investigated in the study are represented using the designation of 203, 610, 356 and 406, respectively. In terms of the cope details, *d1*, *d2*, *d3* are used to represent the three d_c/D ratios (0.05, 0.10 and 0.15), while *c1*, *c2*, *c3*, *c4* and *c5* are used to represent the five c/h_0 ratios (0.1, 0.25, 0.5, 0.75 and 1.0). For example, Model *203-d1-c3* represents the model constructed using UB203 beam section with a 0.05 d_c/D ratio and a 0.5 c/h_0 ratio.

5.2 General results

The FE results show that the failure mode for all the models is local web buckling including both elastic and inelastic buckling. In total, fifty-seven models were failed by inelastic local web buckling at the coped region. The remaining three models (406-*d1-c5*, 406-*d2-c5*, and 406-*d3-c5*) with the largest c/h_0 ratio (1.0), and the largest d/t_w ratio (56.3) were found failure by elastic local web buckling. Typical inelastic local web buckling failure modes obtained from the FE analyses are shown in Figs. 8a and b, while the typical elastic local web buckling failure mode is shown in Fig. 8c. In the models failed by inelastic local web buckling, nine models (203-*d1-c5*, 203-*d2-c5*, 203-*d3-c5*, 610-*d1-c5*, 610-*d2-c5*, 610-*d3-c5*, 356-*d1-c5*, 356-*d2-c5* and 356-*d3-c5*) showed flexural controlled buckling behaviour, and the other forty-eight

models showed shear controlled buckling behaviour. For the models with the shear controlled buckling failure mode local buckling is initiated at the cope corner and a buckling line in the web occurred at around 45° (relative to a vertical line) as shown in Fig. 8a. However, for those models failed by flexural controlled mode, the local buckling is initiated at the top edge of the cope area and the buckling line in the web was at an angle of about 20° as shown in Fig. 8b. Based on the parametric study results, it was found that the shear controlled inelastic local web buckling failure mode of the FE models occurred when $0.1 \leq c/h_0 \leq 0.75$ irrespective of the values of the d/t_w and d_c/D ratios. On the other hand, the flexural controlled inelastic local web buckling failure mode of the FE models occurred when $c/h_0 = 1.0$ and $d/t_w \leq 42.1$.

The typical load-deflection curves of the four beam sections (UB203, UB356, UB610 and UB406) are shown in Fig. 9. In most models (except those failed by elastic local web buckling), a nonlinear load-deflection response is observed before the maximum applied load is achieved (see Figs. 9a-c). This indicates that yielding of the coped beam section occurs before the development of local web buckling of the coped region. It is also found that for the models failed by shear controlled inelastic local web buckling more significant nonlinear load deflection response than those failed by flexural controlled inelastic local web buckling is observed.

5.3 Influence of initial imperfection

In the FE validation, the employed initial imperfection was varied from 0.7mm to 3.0mm. Thus, it is necessary to define a consistent and reasonable initial imperfection at the beginning of the parametric study. The influence of the initial imperfection was examined using models 203-*d3-c3* ($c/h_0 = 0.5$, $d_c/D = 0.15$ and $d/t_w = 26.9$), 610-*d3-c3* ($c/h_0 = 0.5$, $d_c/D = 0.15$ and $d/t_w = 38.3$), 356-*d3-c3* ($c/h_0 = 0.5$, $d_c/D = 0.15$ and $d/t_w = 42.1$) and 406-*d3-c3* ($c/h_0 = 0.5$, $d_c/D = 0.15$ and $d/t_w = 56.3$). It is believed that the selected models are able to represent a typical coped beam configuration with slender and stocky web slenderness. Similar to the FE

validation, a typical first buckling mode obtained from the buckling analysis was employed as the initial imperfection shape. For each model, nonlinear analysis was performed using five imperfection levels of 0.7mm, 1.5mm, 2.5mm, 3.5mm and 4.0mm.

The load-deflection curves of the four models with varying initial imperfection magnitudes obtained from the FE analyses are presented in Fig. 10. It is observed that the initial stiffness of the load-deflection curves obtained using different initial imperfection magnitudes is almost identical. This indicates that the influence of the initial imperfection on the load-deflection behaviour is limited in the elastic stage. However, the influence tends to be more evident in the inelastic stage of the load-deflection behaviour of the models, where the tangent stiffness of both models decreases with increasing initial imperfection. It can also be seen from the figure that the ultimate load decreases with increasing initial imperfection. For the model with stocky web (i.e. 203-*d3*-*c3*) the ultimate load is decreased by 16% when the initial imperfection is increased from 0.7mm to 2.5mm (Fig. 11). However, the ultimate loads of the coped beam models only decrease slightly when the initial imperfection increases beyond 2.5mm as shown in Fig. 11. For the models with the largest slenderness (i.e. 406-*d3*-*c3*), the ultimate load decreases more significantly with increasing imperfection when compared with that of the stocky model (Fig. 11). In general, the ultimate loads of slender coped beams are affected more by the initial imperfection when compared with those of stocky coped beams. Based on the above results, it can be seen that the effect of initial imperfection on the ultimate load of the coped beam models is not significant when its magnitude is larger than 2.5mm. Therefore, a value of 2.5mm is selected as the consistent initial imperfection magnitude used in the parametric studies.

5.4 Influence of cope length to reduced beam depth ratio (c/h_0)

The effect of the cope length to reduced beam depth ratio, c/h_0, on the ultimate reactions of the four beam sections UB203, UB610, UB356 and UB406 with d_c/D ratios of 0.05, 0.10 and 0.15

is shown in Figs. 12a, b, c and d, respectively. The ultimate end plate reaction R_u is given by, $R_u = P_u \times l_d$, where P_u is the ultimate applied load obtained from the FE result, and l_d (1.5D) is the distance from the loading position to the end plate of each beam section. For the models with UB203 section, the ultimate reactions are reduced by 52% (d_c/D = 0.05), 50% (d_c/D = 0.10), and 51% (d_c/D = 0.15) when the c/h_0 ratio is increased from 0.1 to 1.0. For the models with UB406 section, the ultimate reactions are reduced by 54% (d_c/D = 0.05), 61% (d_c/D = 0.10), and 62% (d_c/D = 0.15) when the c/h_0 ratio is increased from 0.1 to 1.0. For the models with other two sections (UB356 and UB610), the ultimate reactions decrease by up to 59% when the c/h_0 ratio is increased from 0.1 to 1.0. Clearly, the ultimate reactions for different beam sections decrease consistently with increasing c/h_0 ratios, although the variation between each section is slightly different. In addition, it can be observed that an almost linear relationship exists between the ultimate reactions and the c/h_0 ratio irrespective of the d_c/D ratio. To further reveal the effect of the ratio of c/h_0 on the beam local web buckling behaviour, the shear stress distribution is investigated at the initial stage of buckling at the coped end. The shear stress distribution of three UB356 models and three UB610 models with a constant d_c/D ratio of 0.1 and varied c/h_0 ratios (0.1, 0.25 and 1.0) are plotted in Fig 13, respectively. For models with small c/h_0 ratios (i.e. 0.1 and 0.25), significant shear stress is found almost fully across the reduced beam depth in the coped area. Significant shear stress is also observed in the buckling area with a clear inclination (larger than 20°), which indicates the location of the buckling line. For models with large c/h_0 ratio (i.e. 1.0), significant shear stress is found across the reduced beam depth only at the end of cope. It is clearly shown that substantial shear yielding governs the failure mode for models with c/h_0 ratio smaller than 1.0.

5.5 Influence of cope depth to beam depth ratio d_c/D

The effect of d_c/D ratio on the local web buckling strength of the coped beam models can also be observed from Figs. 12a-d. As shown in the figures, for the same c/h_0 ratio the ultimate

reaction force decreases with increasing d_c/D ratio. However, the reduction of the reaction force is not significant except for the models with UB406 sections (which is the most slender section of universal beams). For the UB406 section models (Fig. 12d) with a c/h_0 of 0.25, the ultimate reaction decreases significantly from 402kN to 319kN, which represents about 21% reduction, when the d_c/D ratio is increased from 0.05 to 0.15. This indicates that the influence of d_c/D ratio is more substantial for the slender (large d/t_w ratio) beam sections. The decrease of the ultimate reaction for models with a larger d_c/D ratio is probably due to fact that when d_c is increased, the restraint to the top edge of the coped web provided by the beam top flange is reduced, and hence web twisting is more prone to occur. The section reduction caused by the increase of cope depth could also attribute to the decrease of loading capacity. To further examine the effect of d_c/D ratio, shear stress distribution is investigated at the initial stage of buckling at the coped end. The shear stress distributions for three UB203 and three UB406 models with a constant c/h_0 ratio of 0.25 and varied d_c/D ratio (0.05, 0.10 and 0.15) are plotted in Fig 14, respectively. In general, significant shear stress is found across the reduced beam depth in the coped area for all the models. For UB203 models with small d/t_w ratio (26.9), significant shear stress is also found in the buckling area with a clear inclination. Besides, it is observed that the difference of the shear stress distribution for the same beam section with varied d_c/D ratio is relatively small.

6. Design considerations

6.1 Comparison between FE results and current design predictions

As mentioned, the design capacity (R_{design}) was obtained using the lowest values of R_{cr} (either R_{cheng} or R_{yam}), R_{vy} and R_y. In total, the forty-eight FE models which are failed by shear controlled inelastic local web buckling were considered in this section. Table 5 shows the comparisons between the FE results and the design predictions. It was found that the ratio of the FE ultimate reaction to the design capacity (R_u/R_{design}) varies between 0.65 and 1.25 with a

mean value of 0.96 and a corresponding coefficient of variation (CoV) of 0.16. The largest ratio of 1.25 is found in model 610-*d3-c5*, while the lowest ratio of 0.65 is found in model 406-*d1-c3*. Table 5 also shows the mean value and CoV value for different beam sections (UB203, UB610, UB356 and UB406) and for the total forty-eight models. It is observed that, for the UB203 and UB610 models, the R_u/R_{design} ratio is generally larger than unity with a mean value of 1.05 and 1.08, and the corresponding CoV of 0.12 and 0.11, respectively. For UB356 and UB406 models, the average R_u/R_{design} ratio is between 0.90 and 0.79 with a CoV of 0.09 and 0.11, respectively. Hence, it can be seen that the current design method provided inconsistent predictions of the local capacity of coped beams if the beams are failed in inelastic local web buckling mode.

In order to further illustrate the comparisons between the FE results and current design predictions, the normalised buckling strengths of the FE models with varying slenderness parameter are plotted in Fig. 15. As shown in Fig.15a, the ultimate reactions, R_u, of the models failed by shear controlled inelastic local web buckling is normalised by the shear yielding strength, $R_{vy} = 0.6 f_y h_0 t_w$, of the coped section. While for those failed by bending controlled inelastic local web buckling, the maximum bending moment at the end of cope M_u is normalised by the yield moment M_y (Fig.15b), where $M_y = f_y S$, (S = the elastic section modulus of the tee section). The slenderness parameter is defined as the ratio of yield strength to the elastic critical buckling strength [26]. In the case of shear controlled inelastic local web buckling, the shear slenderness parameter is expressed by $\lambda_s = \sqrt{\tau_y / \tau_{cr}}$, where τ_{cr} is the critical shear stress from Eq.(2) proposed by Yam et al. [17], and τ_y is the material shear yield strength, $\tau_y = \sigma_y / \sqrt{3}$. On the other hand, the flexural slenderness parameter for the flexural controlled inelastic local web buckling is expressed by $\lambda_b = \sqrt{f_y / \sigma_{cr}}$, where σ_{cr} is the elastic buckling stress from Eq. (1) based on Cheng's model using the theory of plate buckling [1]. It

can been seen in Figs.15a and b that the maximum R_u/R_{vy} ratio of 1.12 is achieved in model with a d/t_w ratio of 26.9, and a maximum M_u/M_y ratio of 1.25 is achieved in model with a d/t_w ratio of 38.3. More importantly, it is observed in Fig. 15a that the R_u/R_{vy} ratios are generally below the predicted values based on either shear yielding or elastic buckling On the other hand, the M_u/M_y ratios are generally greater than 1.0 as shown in Fig.15b.

Hence, based on the above discussion it can been seen that the current design strategy of evaluating the local strength of coped beam end based on the minimum of the bending yield strength, shear yield strength and elastic local web buckling strength of the coped section may not be appropriate when inelastic local web buckling occurs. Therefore, a design methodology to consider the inelastic local web buckling strength of coped beams is required. In particular, for practical cope details (i.e. where d_c and c are not very large) shear web buckling tends to control the design as illustrated in [17]. Therefore, a design methodology is proposed in the current study to consider the inelastic local web buckling of coped beams based on the shear plate buckling equation. The detail development of the proposed design equations is presented in the following section.

6.2 Proposed inelastic buckling equation

Bleich [26] proposed an equation for evaluating the critical stress of a flat rectangular plate under uniform compressive stress in either the elastic or inelastic range. The inelastic buckling stress (σ_{ie}) can be expressed as:

$$\sigma_{ie} = \eta \frac{k\pi^2 E}{12\left(1-v^2\right)}\left(\frac{t}{b}\right)^2 \tag{6}$$

where E_t is the tangent modulus, E is the Young's modulus, t is the plate thickness and υ is the Poisson's ratio, $\eta = \sqrt{E_t / E}$ is the plasticity reduction factor to account for the inelastic behaviour, k is the buckling coefficient and b is the plate width. Eq. (6) shows that the

inelastic local buckling stress can be obtained by multiplying the elastic local buckling stress by the plasticity reduction factor η. Thus, the inelastic buckling stress can be rewritten by:

$$\sigma_{ie} = \eta \sigma_{cr} \tag{7}$$

where σ_{cr} is the elastic buckling stress.

Past research on top flange coped beams showed that the buckling line in the web usually occurred at an angle of about 45° from a vertical line, particularly for the beams with small c/h_0 ratios. In addition, it was pointed out by Yam et al. [16] that the plate shear buckling model could provide more reasonable predictions for the elastic local web buckling of top flange coped beams compared with that of the classical plate buckling model.

The inelastic shear buckling stress (τ_{ie}) can be obtained by substituting τ_{ie} and τ_{cr} for σ_{ie} and σ_{cr} in Eq. (7).

$$\tau_{ie} = \eta \tau_{cr} \tag{8}$$

where τ_{cr} is the elastic shear buckling stress. For top flange coped beams the elastic shear buckling stress, τ_{cr}, is given in Eq. (3) as proposed in [17]. By rearranging the above equation Eq. (8), the plasticity reduction factor, η, is given in the following form:

$$\eta = \frac{\tau_{ie}}{\tau_{cr}} \tag{9}$$

Accordingly, the inelastic shear buckling stress (τ_{ie}) can be obtained from the FE results and the plasticity reduction factor is then evaluated for each FE model based on Eq. (9). The plot of the plasticity reduction factor η versus the shear slenderness parameter λ_s is shown in Fig. 16. As expected, the reduction factor η increases with the increasing slenderness λ_s. As shown in the figure, a regression analysis using a power function is employed to fit the FE data The

curve fitting produces a coefficient of determination (R^2) of = 0.9768. Hence, the plasticity reduction factor can be evaluated by:

$$\eta = 0.623\lambda_s^{1.51} \tag{10}$$

It should be noted that the above prediction of η is based on the average value of the FE results (shear controlled inelastic buckling models). As shown in Fig. 16, an additional curve is proposed to provide a lower bound of the reduction factor for all the considered FE models. The lower bound reduction factor is given by:

$$\eta = 0.51\lambda_s^{1.5} \tag{11}$$

Therefore, by substituting the proposed plasticity reduction factor to Eq. (8), the inelastic shear stress can be expressed as:

$$\tau_{ie} = 0.623\lambda_s^{1.51} \cdot \tau_{cr} = 0.623\lambda_s^{1.51} \cdot k_s \frac{\pi^2 E}{12(1-\upsilon^2)} \cdot \left(\frac{t_w}{h_0}\right)^2 \tag{12}$$

Conservatively, τ_{ie} can be given by:

$$\tau_{ie} = 0.51\lambda_s^{1.5} \cdot \tau_{cr} = 0.51\lambda_s^{1.5} \cdot k_s \frac{\pi^2 E}{12(1-\upsilon^2)} \cdot \left(\frac{t_w}{h_0}\right)^2 \tag{13}$$

6.3 Proposed design approach

The proposed design equations (Eq. (12) and (13)) for evaluating the inelastic local web buckling strength of top flange coped beams are included in the plot of the normalised ultimate reactions (R_u/R_{vy}) versus the shear slenderness parameter (λ_s) as shown in Fig. 17. As shown in the figure, for $\lambda_s \leq 0.38$ (stocky section) the normalised strength is governed by shear yielding failure whereas for $\lambda_s \geq 1.38$ (slender section) elastic buckling of the coped section controls. The failure of the coped beams is dominated by inelastic local web buckling

for sections with slenderness within the range of $0.38 \leq \lambda_s \leq 1.38$ inelastic local web buckling controls the strength of the coped section. Eq. (12) is recommended for evaluating the inelastic local web buckling strength of top flange coped beams, however, for conservative predictions, Eq. (13) can be used.

In order to investigate the applicability of the proposed design equations, the current design predictions (R_{design}) and the proposed design predictions ($R_{ie,av}$ and $R_{ie,con}$) are compared with the test results (R_{ex}) [1, 8], respectively in Table 6. Clearly, the test-to-predicted ratio (R_{ex}/R_{design}) obtained according to the current design equation is generally smaller than unity, with a mean value of 0.87 and a CoV of 0.12. It indicates that the current design equation could not offer a safe and consistent prediction for the top flange coped beam failed by inelastic local web buckling. On the other hand, using the proposed design curve Eq. (12), the average test-to-predicted ratio ($R_{ex}/R_{ie,av}$) for all the considered test results is 1.18, and the corresponding CoV is 0.10. Alternatively, using the lower bound design curve Eq. (13), the average test-to-predicted ratio ($R_{ex}/R_{ie,cov}$) is 1.44, with an associated CoV of 0.10. Based on the above, it can be seen that proposed design equation Eq. (12) provides reasonable estimates of the inelastic buckling strength of the top flange coped beam specimens. It should be noted that the proposed design equations are only applicable for evaluating the local strength of top flange coped beams with d/t_w ratio between 26.9 and 56.3, $c/h_o < 1.0$, $d_c/D < 0.15$ and a welded end-plate connection. However, it is believed that the range of beam sections and cope details examined in this study are able to cover most of the practical dimensions of coped beam connections.

7. Summary and conclusions

In this paper, the inelastic behaviour of top flange coped beams was investigated through a comprehensive numerical study using the FE method. Firstly, a FE model was developed and validated by existing test results [1, 8]. The test-to-FE ratio of the ultimate strength of the

specimens (R_{ex}/R_{nu}) ranged from 0.96 to 1.03 with an average value of 0.99 and an associated CoV of 0.024.

Subsequently, a parametric study was performed based on the validated FE model. The effects of various parameters including the coped details, the web slenderness and the initial geometric imperfection on the structural behaviour of top flange coped beams were examined. A total of sixty FE analyses were carried out in the study. Evident inelastic local web buckling behaviour was observed in fifty-seven models. Three models (406-*d1*-*c5*, 406-*d2*-*c5* and 406-*d3*-*c5*) with the largest d/t_w ratio and c/h_0 ratio were failed by elastic local web buckling. Two different inelastic failure modes related to the inclination of the buckling line were observed in the analyses. Forty-eight models were failed by shear controlled inelastic local web buckling, while nine models were found failure by flexural controlled inelastic local web buckling. The numerical study also showed that increasing the c/h_0 ratio reduced the ultimate reaction of the coped beams. Increasing d_c/D ratio also led to the reduction of the ultimate reaction, however, the influence of which is not as remarkable as that of the c/h_0 ratio.

The parametric analysis results were compared with the predictions based on the current design strategy. It was found that the existing design strategy could not provide consistent predictions of the inelastic buckling strength of coped beams. Hence, an alternative new design approach was proposed to enhance the design accuracy and efficiency. This approach was based on the 'plate shear buckling' equation where the inelastic buckling stress was predicted using the elastic shear bucking stress τ_{cr} [17] multiplied by a plasticity reduction factor η. This reduction factor was related to the non-dimensional slenderness $\lambda_s = \sqrt{\tau_y / \tau_{cr}}$ and was obtained using a regression analysis of the numerical results. The inelastic web buckling strengths of the coped beam specimens predicted by the proposed approach are in

reasonable agreement with the existing test results [1, 8]. The average test-to-predicted ratio of the ultimate strength is 1.18 with an associated CoV of 0.10.

Acknowledgement

The work presented in this paper is partially supported by the Hong Kong Polytechnic University Central Research Grant (Project No. G-YBCF).

References

[1] Cheng JJR, Yura JA, Johnson CP. Design and behaviour of coped beams. Ferguson structural Engineering Laboratory, Department of Civil Engineering, University of Texas at Austin 1984;Report No.84-1.

[2] Ricles JM, Yura JA. The behaviour and analysis of double-row bolted shear web connections. Ferguson structural Engineering Laboratory, Department of Civil Engineering, University of Texas at Austin 1980;Phil. M. Thesis No. 80-1.

[3] Birkemoe PC, Gilmor MI. Behavior of bearing critical double-angle beam connections. Eng J Am Inst Steel Constr 1978;15:109-15.

[4] Shelton BG, Yura JA. Tests of bolted shear web connections. Ferguson structural Engineering Laboratory, Department of Civil Engineering, University of Texas at Austin 1981;Report No. 81-1.

[5] Ricles JM, Yura JA. Strength of double-row bolted-web connections. J Struct Eng 1983;109:126-42.

[6] Yura JA, Birkemoe PC, Ricles JM. Beam web shear connections: an experimental study. ASCE J Struct Div 1982;108:311-25.

[7] Cheng JJR, Yura JA. Local web buckling of coped beams. J Struct Eng 1986;112:2314-31.

[8] Yam MCH, Zhong YC, Lam ACC, Iu VP. An investigation of the block shear strength of coped beams with a welded clip angle connection — Part I: Experimental study. Journal of Constructional Steel Research 2007;63:96-115.

[9] Yam MCH, Zhong YC, Lam ACC, Iu VP. An investigation of the block shear strength of coped beams with a welded clip angle connection — Part II: Numerical study. Journal of Constructional Steel Research 2007;63:116-34.

[10] Fang C, Lam ACC, Yam MCH, Seak KS. Block shear strength of coped beams with single-sided bolted connection. J Constr Steel Res 2013;86:153-66.

[11] Yam MCH, Grondin GY, Wei F, Chung KF. Design for block shear of coped beams with a welded end connection. J Struct Eng 2011;137:811-21.

[12] Wei F, Yam MCH, Chung KF, Grondin GY. Tests on block shear of coped beams with a welded end connection. Journal of Constructional Steel Research 2010;66:1398-410.

[13] Lam ACC, Fang C, Yam MCH, Wang W, Iu VP. Block shear strength and design of coped beams with double bolt-line connections. Eng Struct 2015;100:293-307.

[14] Lam ACC, Yam MCH, Fu CKM. Experimental investigation of the local web buckling strength of coped steel i-beam with and without stiffeners. Real Struct : Bridges Tall Buildings - Proc 10th East Asia-Pacific Conf on Struct Eng Construction, EASEC 2006;4:559-64.

[15] Yam MCH, Ma H, Lam ACC, Chung KF. Experimental study of the strength and behaviour of reinforced coped beams. J Constr Steel Res 2011;67:1749-59.

[16] Yam MCH, Fang C, Lam ACC, Cheng JJR. Local failures of coped steel beams - A state-of-the-art review. J Constr Steel Res 2014;102:217-32.

[17] Yam MCH, Lam ACC, Iu VP, Cheng JJR. Local web buckling strength of coped steel I beams. J Struct Eng 2003;129:3-11.

[18] Aalberg A. Design of aluminium beam ends with flange copes. Thin-Walled Struct 2015;94:593-602.

[19] Aalberg A. Experimental and numerical parametric study on the capacity of coped beam ends. Journal of Constructional Steel Research 2015;113:146-55.

[20] American Institute of Steel Construction (AISC). Steel Construction Manual, One East Wacker Drive, Suite 700, Chicago, Illinois, US: AISC, 2011.

[21] The Steel Construction Institute (SCI), The British Constructional Steelwork Association Limited (BCSA). Joints in Steel Construction: Simple Connections, UK: SCI and BCSA, 2002.

[22] ABAQUS Standard/analysis user's manual, Version 6.12., Providence, RI, USA: Dassault Systèmes Simulia Corp., 2012.

[23] Fisher JW. Fatigue and fracture in steel bridges. Case studies, New York, United States: John Wiley and Sons Ltd., 1984.

[24] Yam MC, Cheng JR. Fatigue strength of coped steel beams. J Struct Eng 1990;116:2447-63.

[25] Khoo XE, Perera M, Albermani F. Design of eccentrically connected cleat plates in connections . International Journal of Advanced Steel Construction 2010;6:678-87.

[26] Bleich F. Buckling strength of metal structures, New York: McGraw-Hill, 1952.

List of Tables

Table 1: Measured dimensions and cope details of test specimens [1, 8]

	Specimen No.	Web thickness	Flange thickness	Beam depth	Flange width	Connected length		Connection position	Cope length	Cope depth	Weld size
		t_w (mm)	T (mm)	D (mm)	B (mm)	a (mm)	b (mm)	p (mm)	c (mm)	d_c (mm)	s_1 (mm)
Cheng et al. [1]	W1	7.7	11.2	453.4	152.4	64	216	25	89	32	5
	W2	7.7	11.2	453.4	152.4	140	216	25	165	32	5
Yam et al. [8]	A1	6.8	11.1	404.2	140.9	50	160	20	100	33	9
	A2	6.8	11.1	404.2	140.9	70	140	20	120	31	9
	B1	6.8	11.1	404.2	140.9	50	120	20	100	30	10
	B2	6.8	11.1	404.2	140.9	90	110	20	130	30	10
	D1	9.2	14.2	456.3	189.1	90	120	20	150	30	12
	E2	9.1	15.2	362.6	171.5	50	120	45	100	30	14

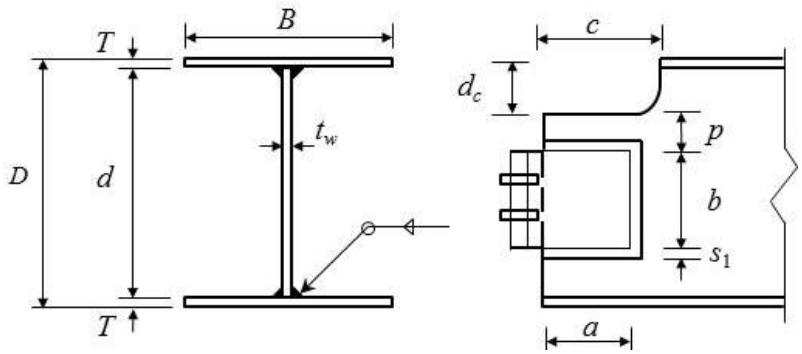

Table 2: Material properties for FE validation [1, 8]

	Specimen No.	Elastic modulus E (GPa)	Yield strength σ_y (MPa)	Ultimate strength σ_u (MPa)
Cheng et al. [1]	W1, W2	200	272	430
Yam et al. [8]	A1, A2	191	319	683
	B1, B2	203	319	683
	D1	203	372	750
	E2	204	305	685
	Clip angle	203	306	760

Table 3: Comparison of FE results with test results [1, 8]

Specimens		Ultimate load (kN)		Ultimate reaction (kN)		Failure mode		$\frac{R_{ex}}{R_{nu}}$	Initial imperfection (mm)
		Test-P_{ex}	FEA-P_{nu}	Test-R_{ex}	FEA-R_{nu}	Test	FEA		
Cheng et al. [1]	W1	-	-	509.5	489.9	ILWB	ILWB	0.96	1.0
	W2	-	-	493.2	482.4	ILWB	ILWB	0.99	1.0
Yam et al. [8]	A1	495.5	505.0	395.2	412.0	ILWB	ILWB	0.96	0.7
	A2	550.1	537.0	437.4	443.6	ILWB	ILWB	0.99	1.7
	B1	500.3	493.0	394.0	406.0	ILWB	ILWB	0.97	3.0
	B2	490.2	481.0	390.3	396.1	ILWB	ILWB	0.99	3.0
	D1	811.0	781.0	623.0	605.0	ILWB	ILWB	1.03	3.0
	E2	756.4	716.2	581.0	576.1	ILWB	ILWB	1.01	3.0
							Mean =	0.99	
							COV =	0.024	

Note: ILWB represents inelastic local web buckling

Table 4: Geometric details of parametric study

Parameters	**UB203×133×30**			**UB610×305×179**			**UB356×171×51**			**UB406×140×39**		
Beam depth, *D* (mm)	206.8			620.2			355.0			398.0		
Beam width, *B* (mm)	133.9			307.1			171.5			141.8		
Depth between fillets, *d* (mm)	172.4			540			311.6			360.4		
Flange thickness, *T* (mm)	9.6			23.6			11.5			8.6		
Web thickness, t_w (mm)	6.4			14.1			7.4			6.4		
d/t_w	26.9			38.3			42.1			56.3		
d_c/D	0.05, 0.1, 0.15			0.05, 0.1, 0.15			0.05, 0.1, 0.15			0.05, 0.1, 0.15		
cope depth, d_c (mm)	11	21	31	31	62	93	18	36	53	20	40	60
$h_0 = D-d_c$ (mm)	196	186	176	587	556	525	338	320	302	378	358	338
c/h_0	0.1, 0.25, 0.5, 0.75, 1.0			0.1, 0.25, 0.5, 0.75, 1.0			0.1, 0.25, 0.5, 0.75, 1.0			0.1, 0.25, 0.5, 0.75, 1.0		

Table 5: Comparisons between FE results and design predictions

$\frac{R_u}{R_{design}}$	**Section No.**	**UB203**	**UB610**	**UB356**	**UB406**	**Total 48**
	Mean	1.05	1.08	0.90	0.79	0.96
	CoV	0.12	0.11	0.09	0.11	0.16

Table 6: Comparisons between test results and predictions from the proposed design equations

	Specimen No.	$\frac{R_{ex}}{R_{design}}$	$\frac{R_{ex}}{R_{ie,av}}$ [Eq. (12)]	$\frac{R_{ex}}{R_{ie,con}}$ [Eq. (13)]
Cheng et al. [1]	W1	1.00	1.16	1.40
	W2	0.97	1.37	1.67
Yam et al. [8]	A1	0.85	1.13	1.38
	A2	0.94	1.32	1.60
	B1	0.84	1.10	1.33
	B2	0.80	1.18	1.44
	D1	0.74	1.00	1.21
	E2	1.09	1.20	1.46
	Mean	0.90	1.18	1.44
	CoV	0.13	0.10	0.10

List of Figures

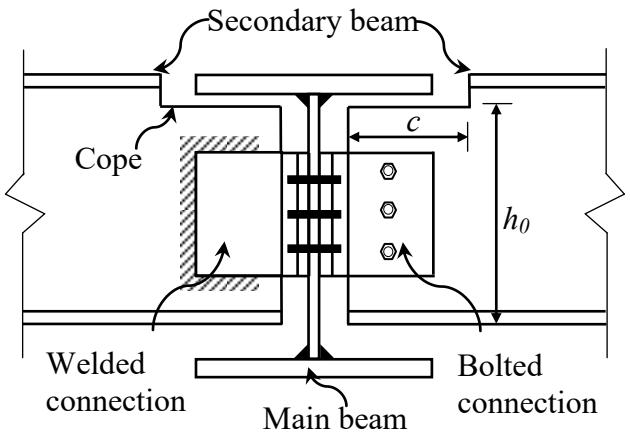

Figure 1: Welded or bolted connection on top flange coped beams

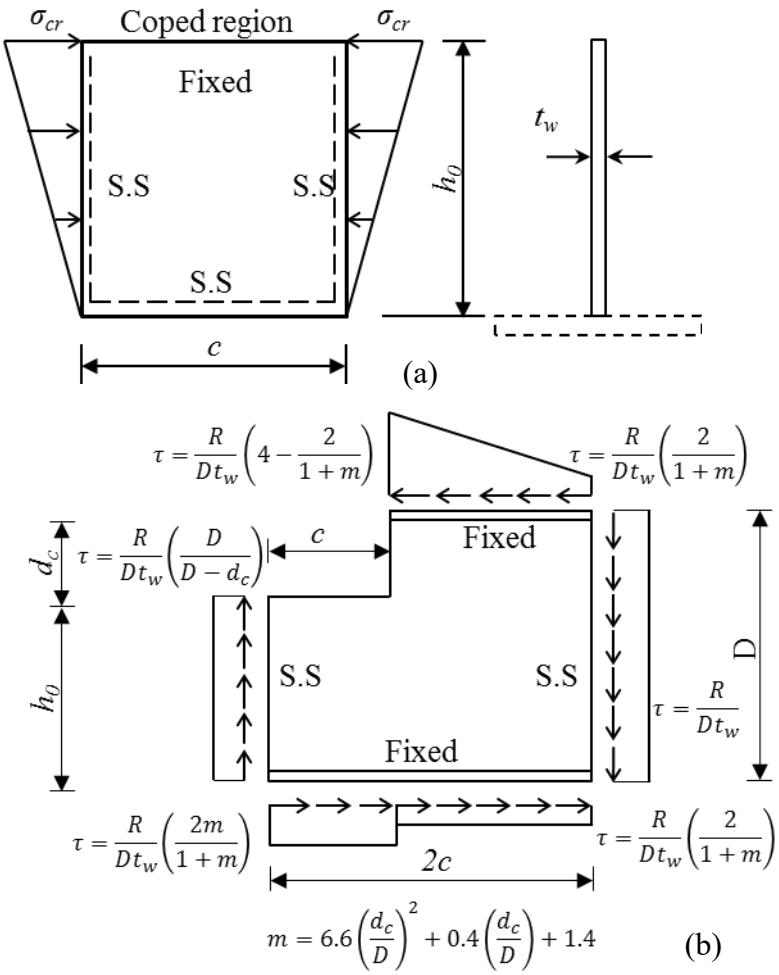

Figure 2: Design models: (a) plate buckling model [1] and (b) plate shear buckling model for local web buckling of top flange coped beams [17]

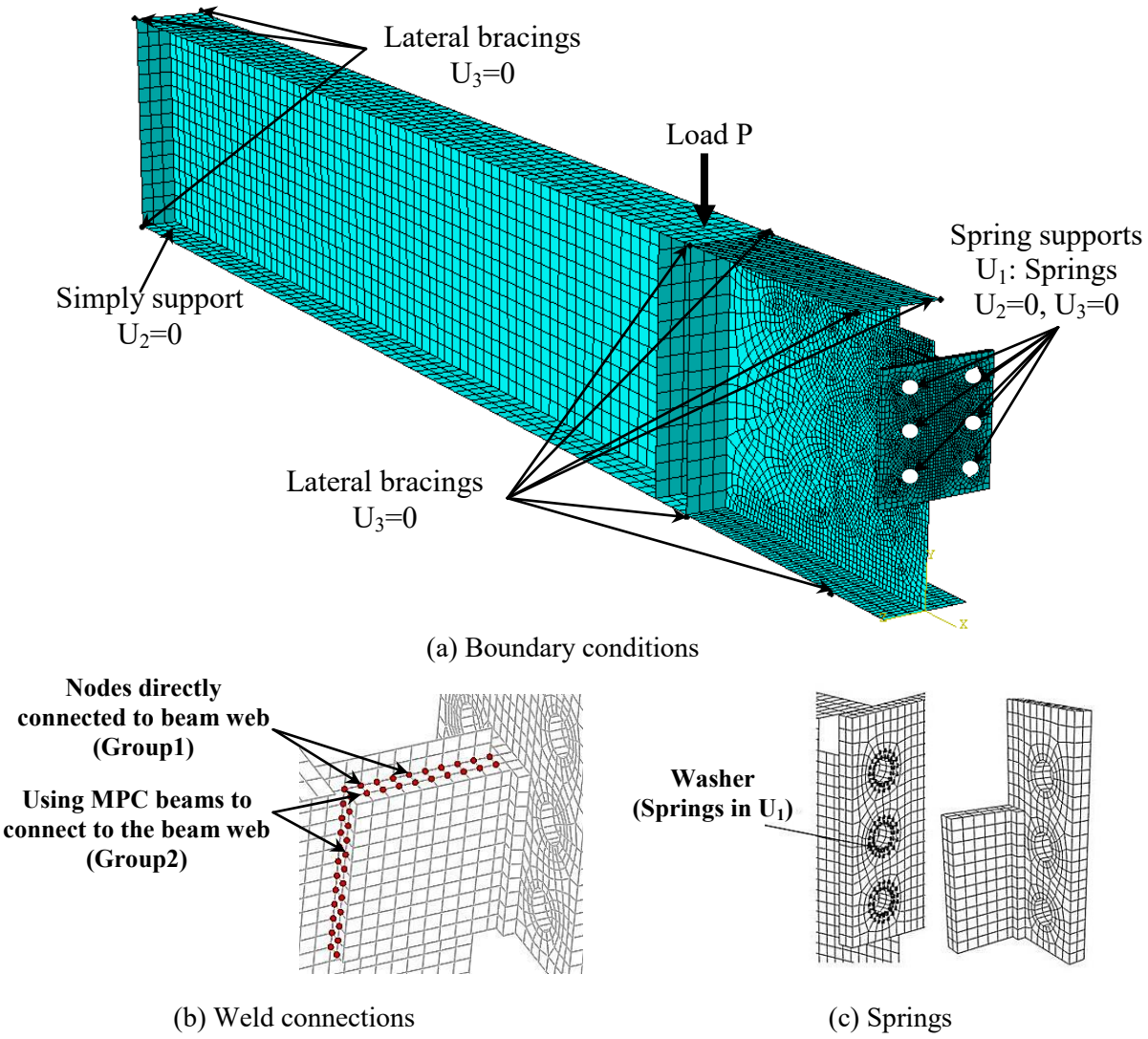

Figure 3: FE models of the test specimens

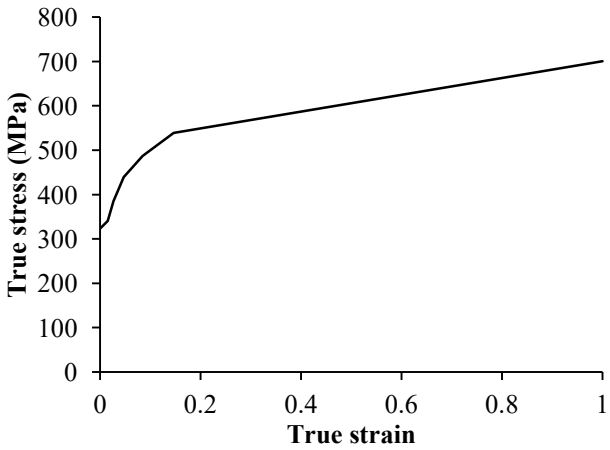

Figure 4: Material model for validation and parametric study

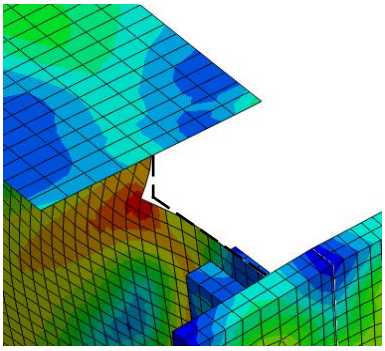

(a) A2-failure mode (FE)

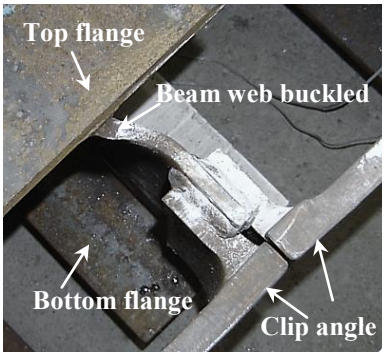

(b) A2-failure mode (Test) [8]

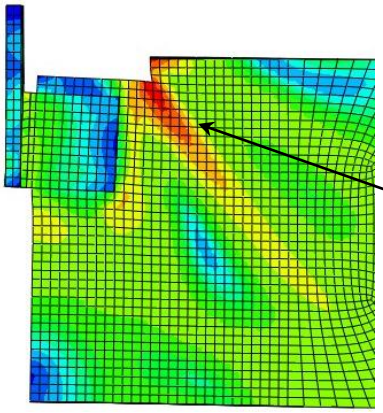

(c) B2-failure mode

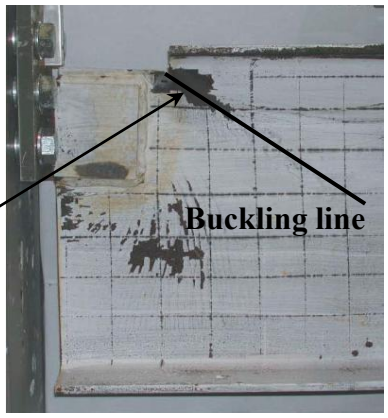

(d) B2-failure mode (Test) [8]

Figure 5: Experimental-numerical comparisons of failure mode

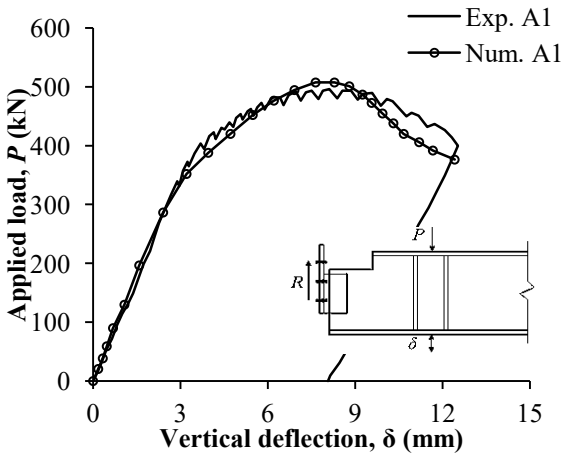

(a) Load-deflection curves of A1

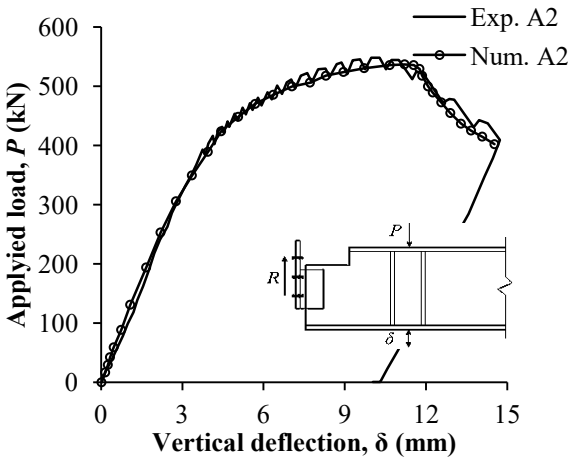

(b) Load-deflection curves of A2

Figure 6: Experimental-numerical comparisons of load-deflection curves (Cont'd)

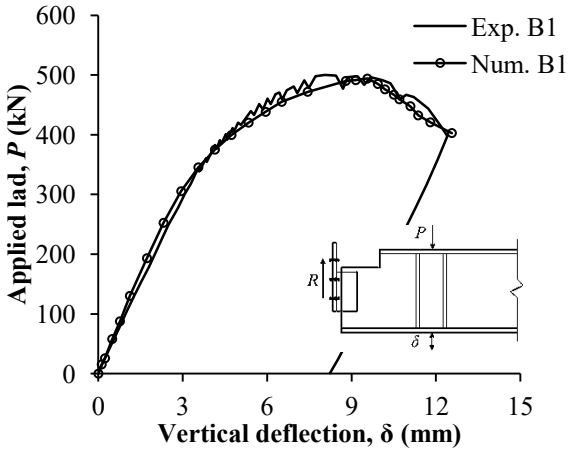

(c) Load-deflection curves of B1

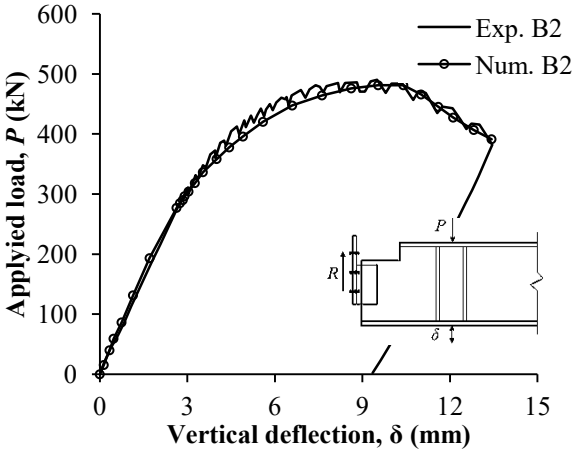

(d) Load-deflection curves of B2

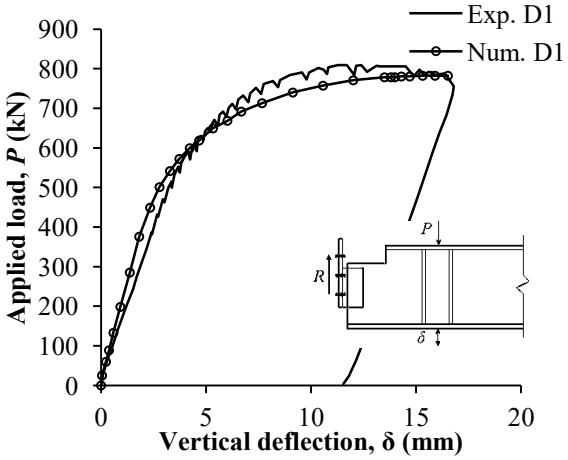

(e) Load-deflection curves of D1

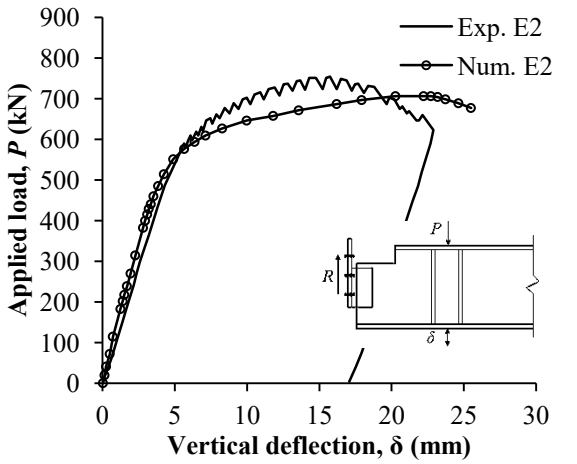

(f) Load-deflection curves of E2

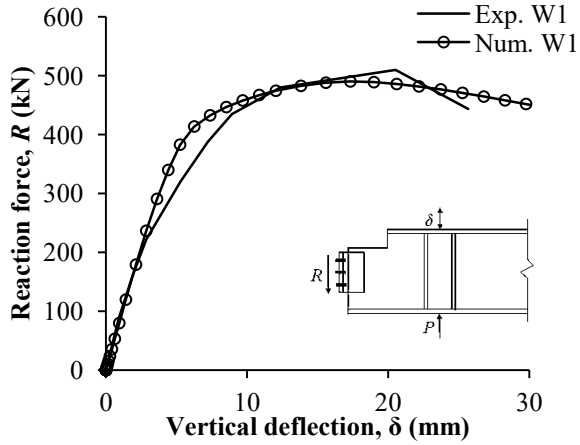

(g) Load-deflection curves of W1

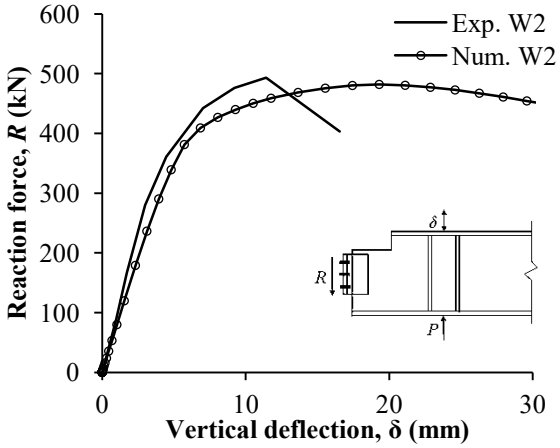

(h) Load-deflection curves of W2

Figure 6: Experimental-numerical comparisons of load-deflection curves

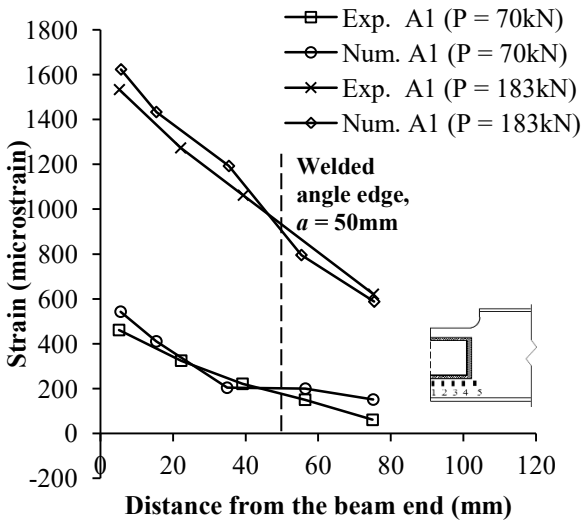

(a) Strain distributions of A1

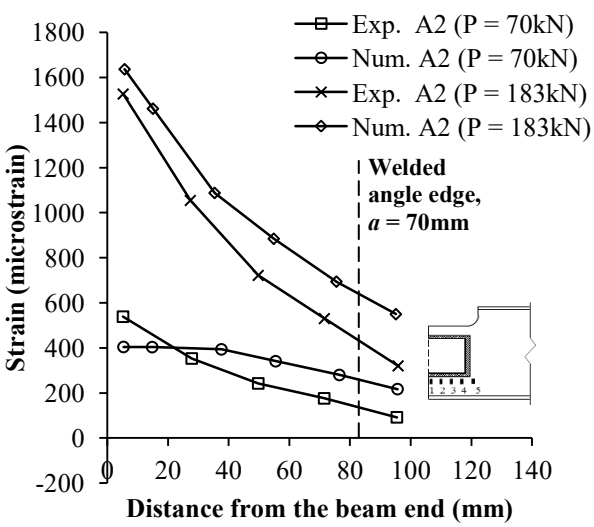

(b) Strain distributions of A2

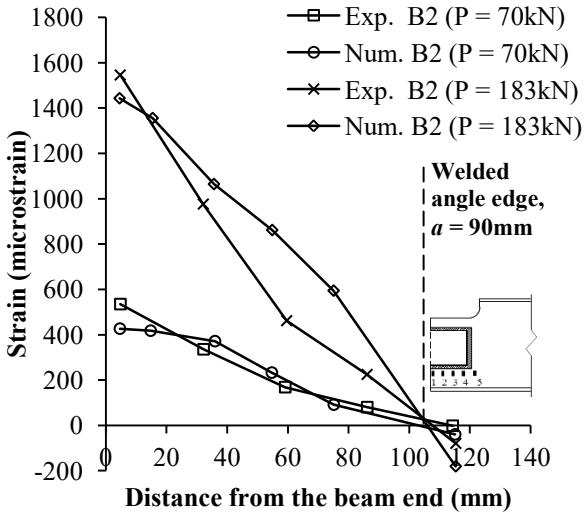

(c) Strain distributions of B2

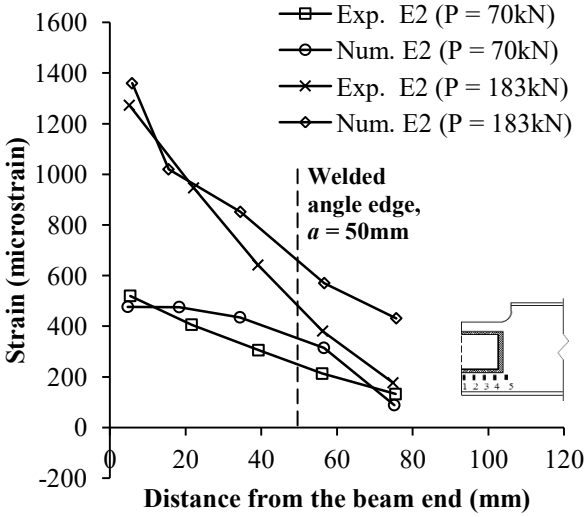

(d) Strain distributions of E2

Figure 7: Numerical-experimental comparisons of strain distributions

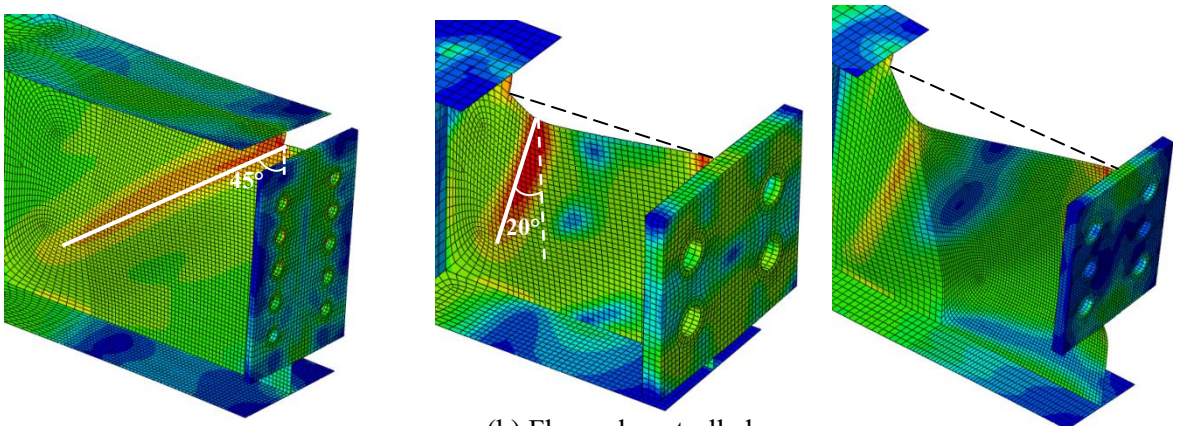

(a) Shear controlled inelastic local web buckling

(b) Flexural controlled inelastic local web buckling

(c) Elastic local web buckling

Figure 8: Typical failure mode (von Mises stress contours) of parametric studies

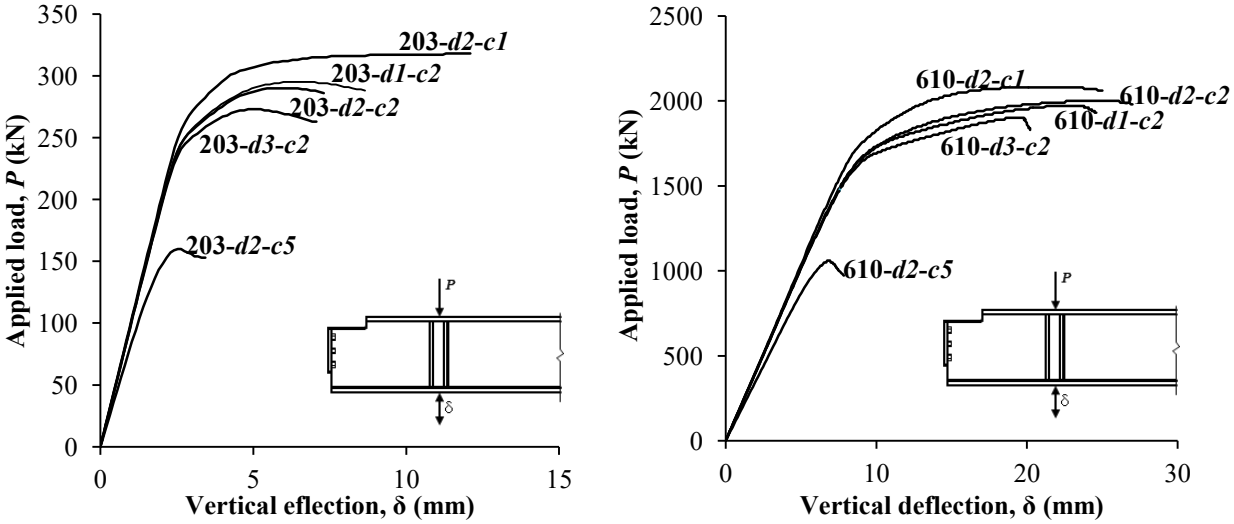

(a) UB203 section (d/t_w = 26.9)

(b) UB610 section (d/t_w = 38.3)

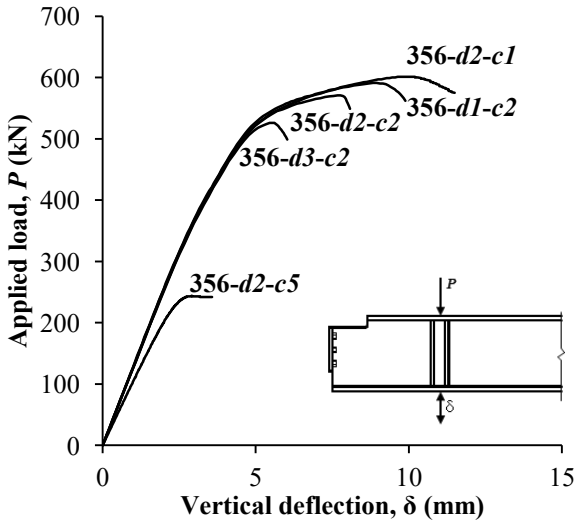

(c) UB356 section (d/t_w = 42.1)

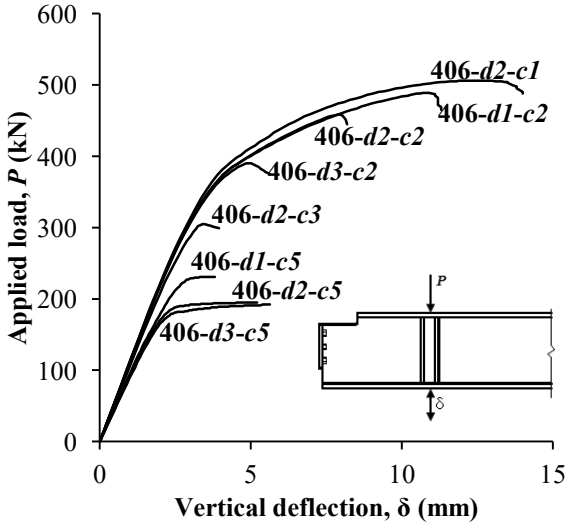

(d) UB406 section (d/t_w = 56.3)

Figure 9: Typical load-deflection curves of different beam sections

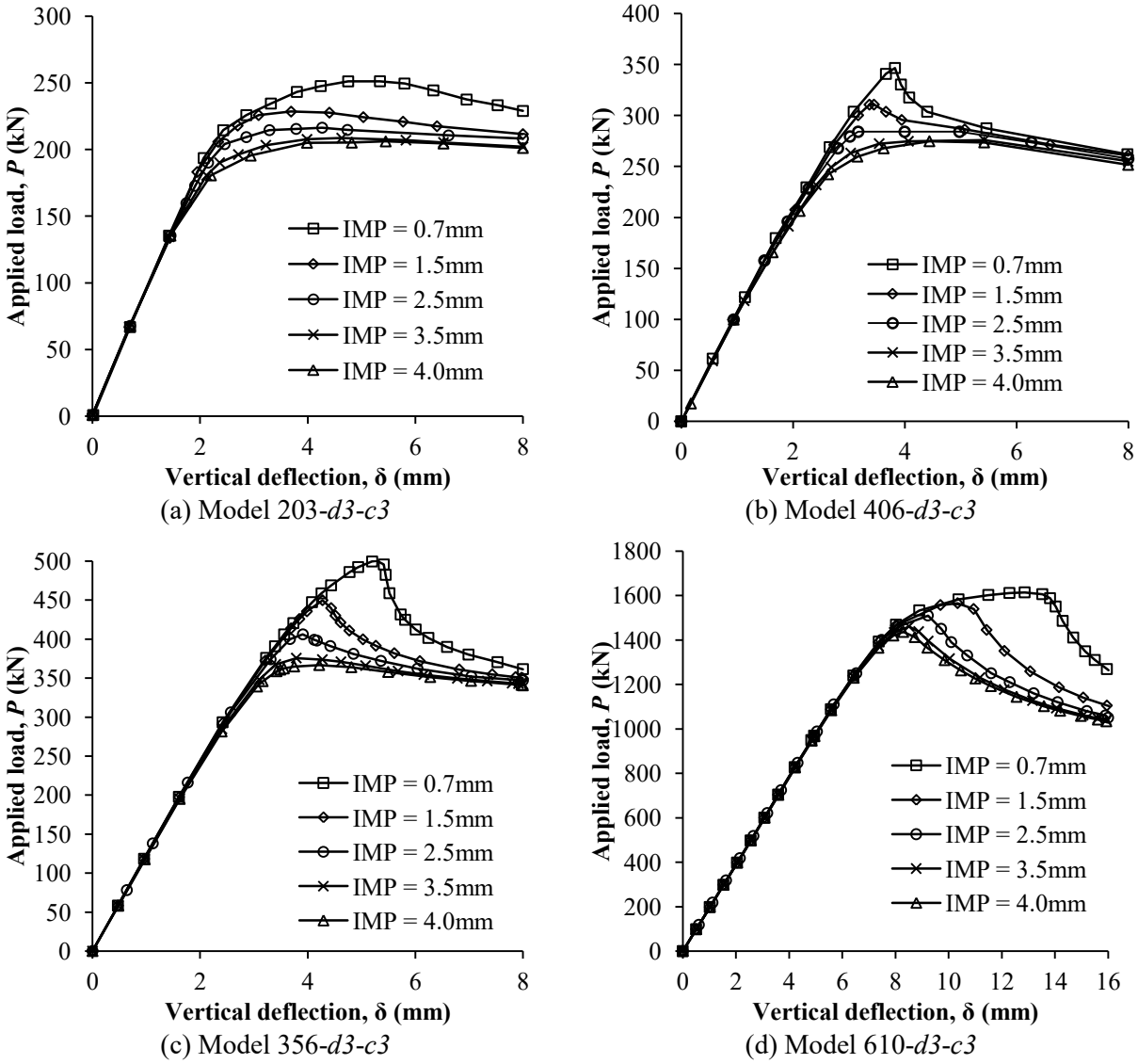

(a) Model 203-*d3-c3*

(b) Model 406-*d3-c3*

(c) Model 356-*d3-c3*

(d) Model 610-*d3-c3*

Figure 10: Load-deflection curves with varied initial imperfection magnitude

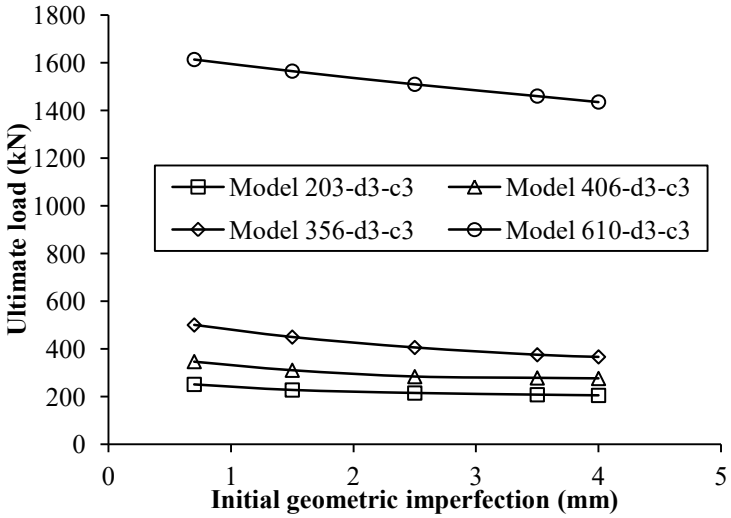

Figure 11: Effect of initial imperfection on the ultimate applied load

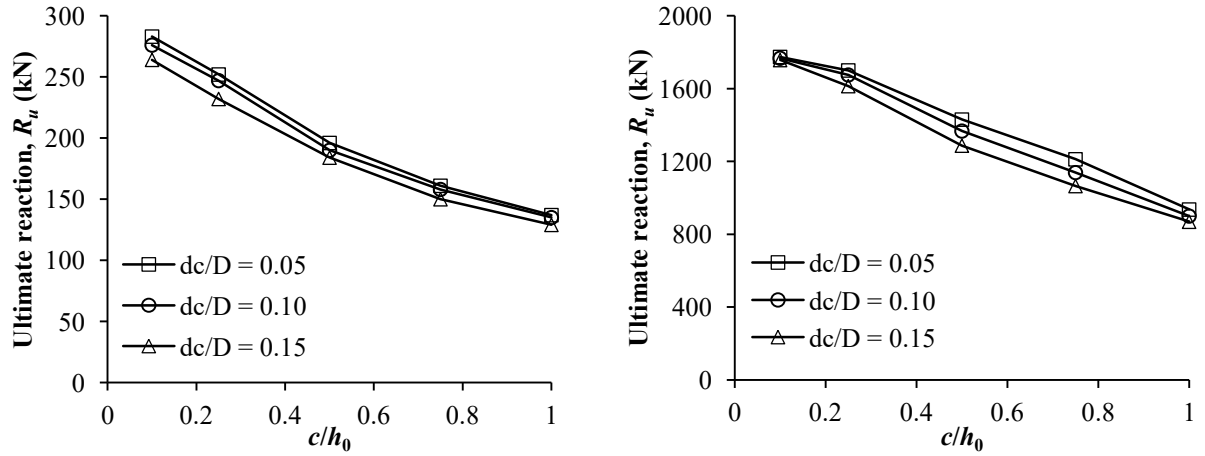

(a) UB203 section (d/t_w = 26.9)

(b) UB610 section (d/t_w = 38.3)

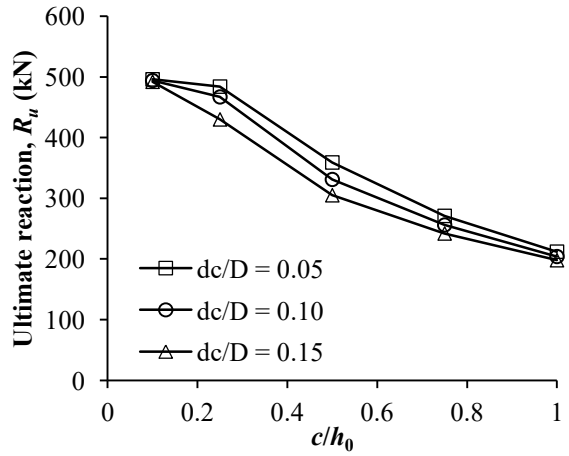

(c) UB356 section (d/t_w = 42.1)

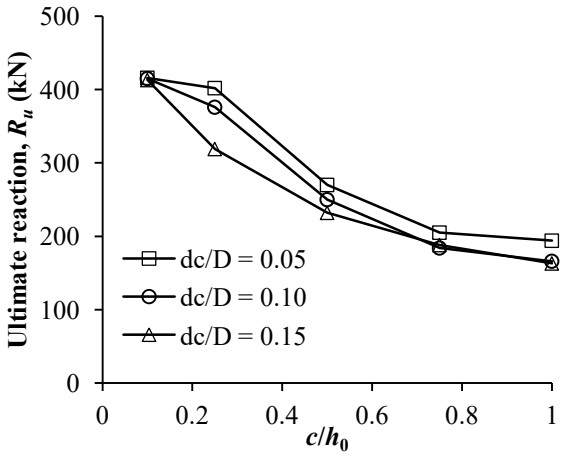

(d) UB406 section (d/t_w = 56.3)

Figure 12: Effect of cope details on the ultimate reaction of different beam sections

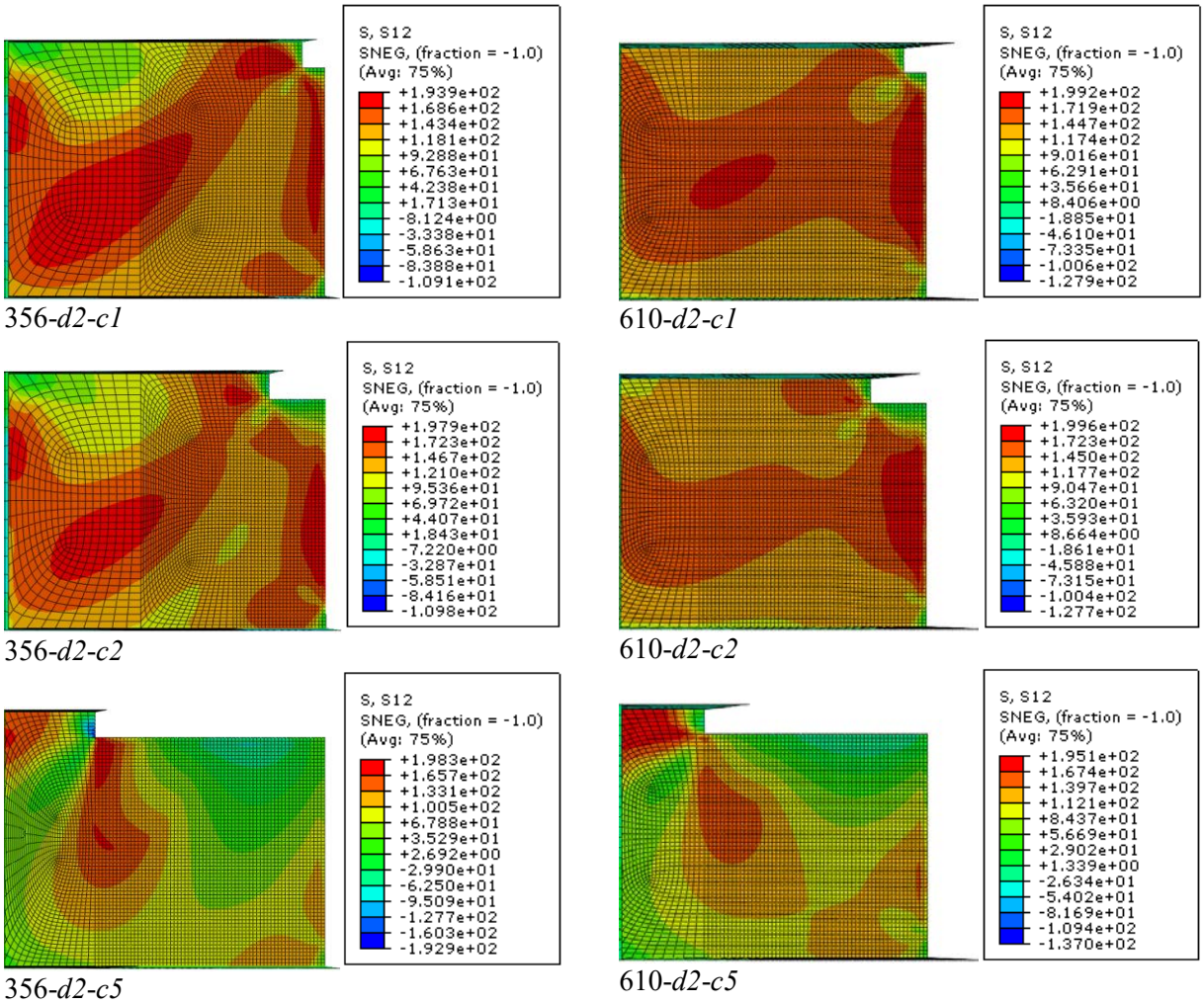

Figure 13: Shear stress distributions for different beam sections with different c/h_0 ratios at the initial stage of buckling

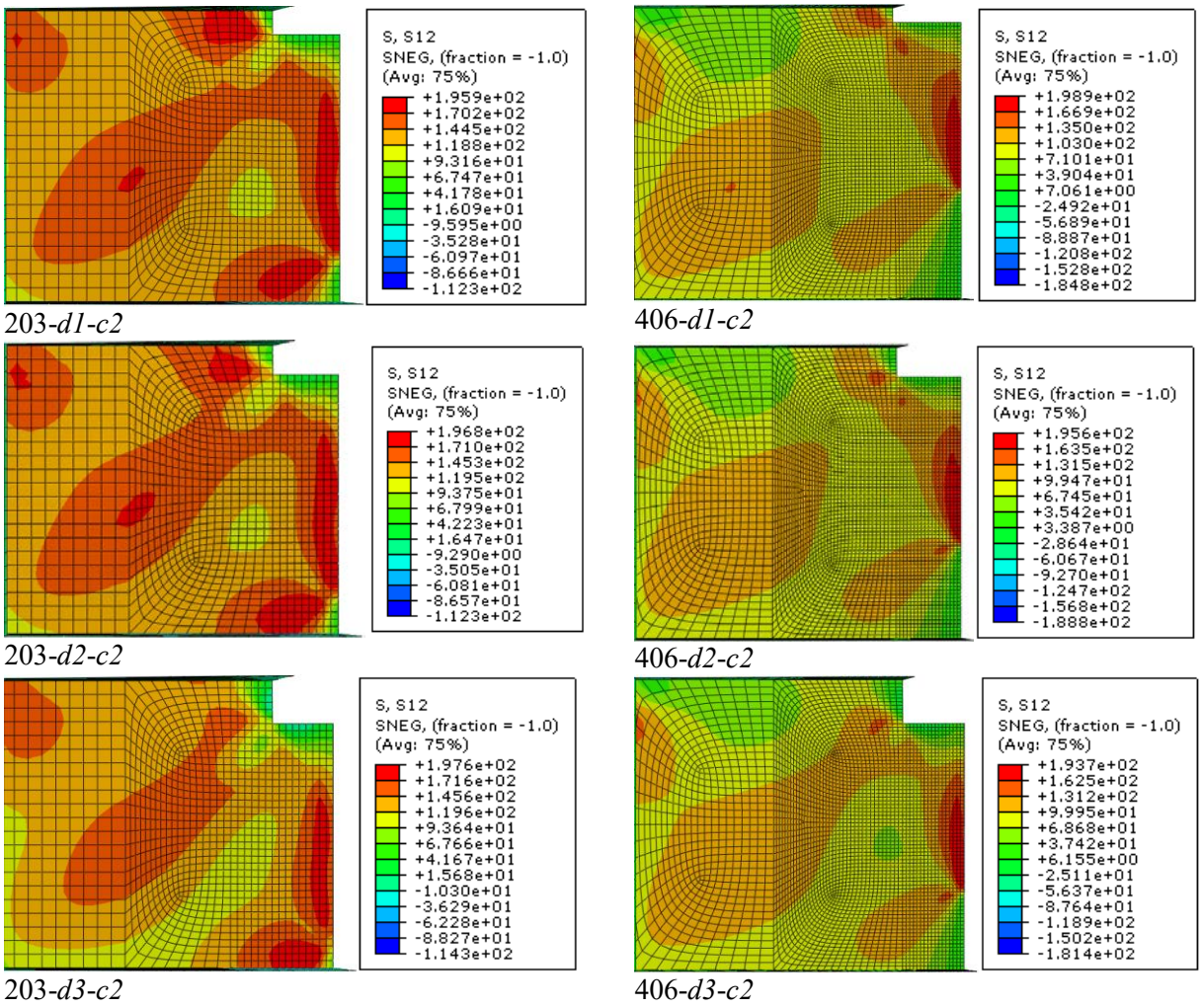

Figure 14: Shear stress distributions for different beam sections with different d_c/D ratios at the initial stage of buckling

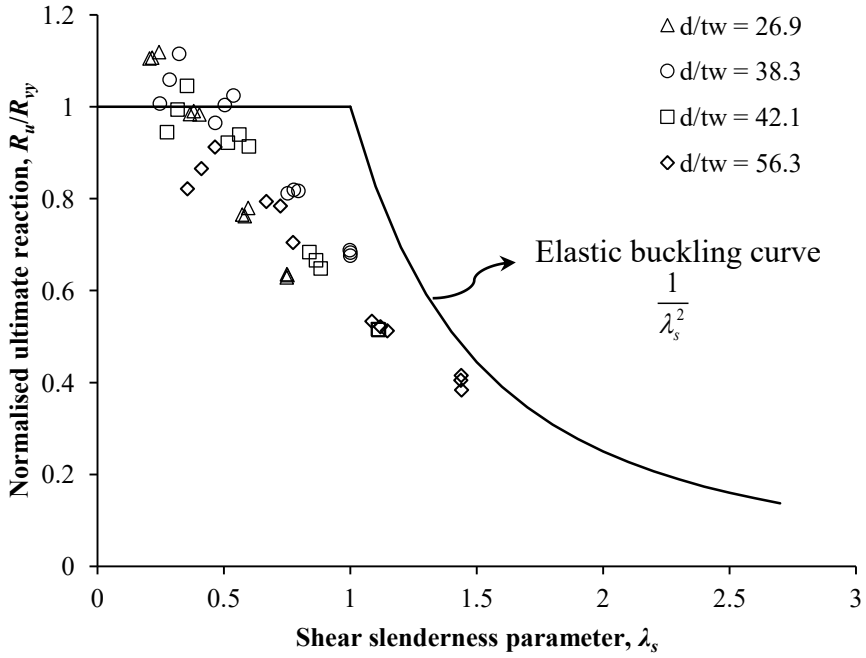

(a) Shear controlled inelastic local web buckling behaviour

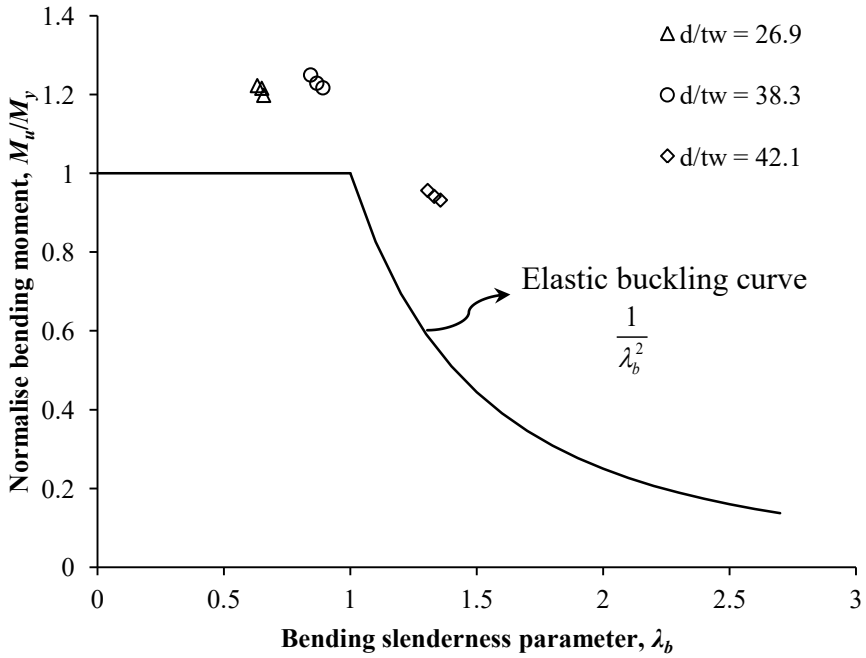

(b) Flexural controlled inelastic local web buckling behaviour

Figure 15: Plots of normalised ultimate reactions/bending moments vs slenderness parameter

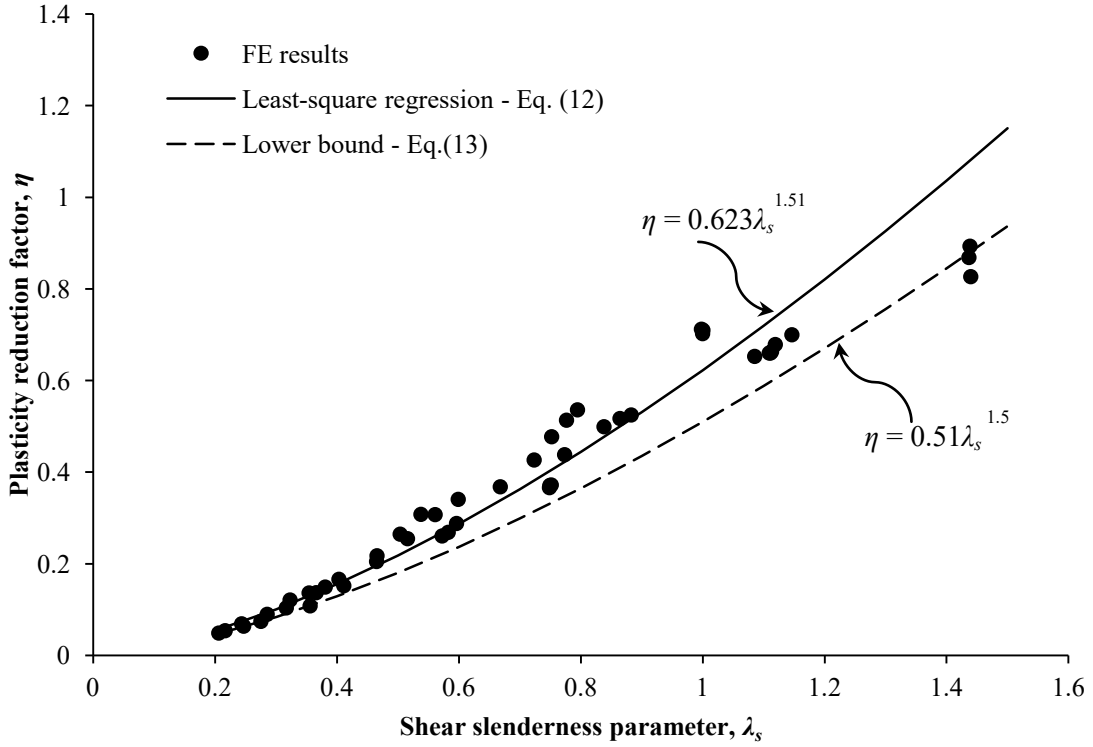

Figure 16: Proposed equations for predicting η

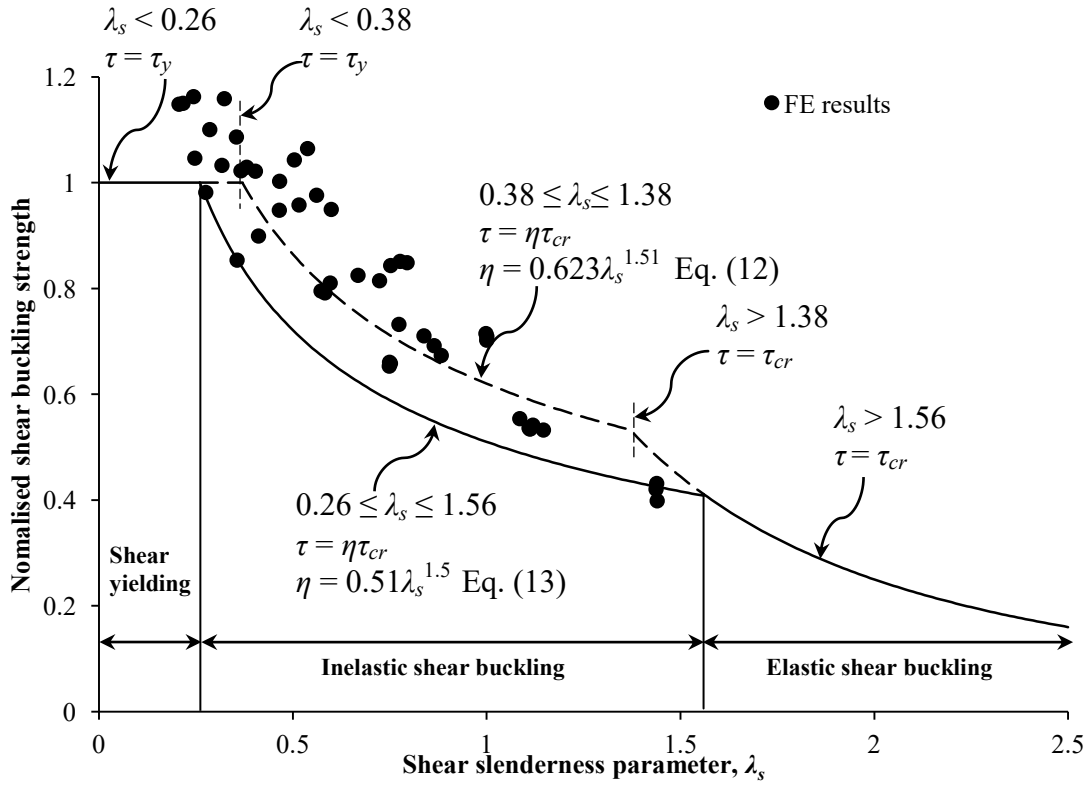

Figure 17: Design approach of local web buckling based on plate shear buckling equation